

A Coupled CP Decomposition for Principal Components Analysis of Symmetric Networks

Michael Weylandt and George Michailidis

Abstract—In a number of application domains, one observes a sequence of network data; for example, repeated measurements between users interactions in social media platforms, financial correlation networks over time, or across subjects, as in multi-subject studies of brain connectivity. One way to analyze such data is by stacking networks into a third-order array or tensor. We propose a principal components analysis (PCA) framework for sequence network data, based on a novel decomposition for semi-symmetric tensors. We derive efficient algorithms for computing our proposed “Coupled CP” decomposition and establish estimation consistency of our approach under an analogue of the spiked covariance model with rates the same as the matrix case up to a logarithmic term. Our framework inherits many of the strengths of classical PCA and is suitable for a wide range of unsupervised learning tasks, including identifying principal networks, isolating meaningful changepoints or outliers across observations, and for characterizing the “variability network” of the most varying edges. Finally, we demonstrate the effectiveness of our proposal on simulated data and on examples from political science and financial economics. The proof techniques used to establish our main consistency results are surprisingly straightforward and may find use in a variety of other matrix and tensor decomposition problems.

Index Terms—Principal components, network analysis, tensor decomposition, semi-symmetric tensors, CP factorization

I. INTRODUCTION

PRINCIPAL Components Analysis (PCA) is a fundamental tool for the analysis of multivariate data, enabling a wide range of dimension reduction, pattern recognition, and visualization strategies [1]. Originally introduced by Pearson and Hotelling for investigating low-dimensional data in a Euclidean space, PCA has been generalized to much more general contexts, including data taking values in (possibly infinite-dimensional) function spaces [2], discrete and compositional spaces [3], and shape spaces [4]. In this work, we propose a novel PCA-type decomposition for *network data*: that is, given a set of undirected networks on a common set of nodes, we seek to identify common patterns in the form of one or more low-rank “principal networks” that capture most of the variation in our data set. Our main technical tool is a *novel tensor decomposition* on so-called “semi-symmetric tensors,” for which we provide an efficient computational algorithm and probabilistic guarantees (consistency result).

Semi-symmetric tensors are third order tensors, *i.e.*, three dimensional arrays, each slice of which along a fixed axis yields a (real) symmetric matrix. By convention, we take

the first two dimensions to be the axes of symmetry, so $\mathcal{X} \in \mathbb{R}^{p \times p \times T}$ is a semi-symmetric tensor if $\mathcal{X}_{\cdot i}$ is a $p \times p$ symmetric matrix for all $1 \leq i \leq T$. Semi-symmetric tensors have been previously successfully applied to the study of brain networks [5], as the basis of a convex formulation of network clustering [6], and in certain medical imaging problems [7], though this work is the first to give theoretical guarantees of the type presented in Theorem 1 below. Kolda [8] considers a similar decomposition framework for fully-symmetric tensors and gives a thorough review of related results in that context.

We take the “canonical polyadic” or “CP” tensor decomposition framework as our starting point. The CP decomposition approximates a tensor by a sum of rank-1 components, which are typically estimated using an alternating least squares approach [9, Section 3]. The CP decomposition has been applied as the basis for various forms of tensor PCA, where it is preferred over Tucker-type decompositions because it provides interpretable and ordered components, similar to those resulting from classical (matrix) PCA [10]. For scalar data arranged in a tensor, CP-based tensor PCA exhibits a strong performance and has been fruitfully extended to sparse and high-dimensional settings with efficient algorithms [11], [12], but it is less ideal for network settings. Specifically, CP-based approaches decompose a tensor into rank-1 components, but realistic networks essentially never have exact rank-1 structure, as this would imply a uniform connectivity pattern across all nodes. This problem—developing a tensor decomposition and PCA framework which outputs meaningful networks—motivates the novel “coupled CP” decomposition at the heart of this paper.

The remainder of this paper is organized as follows: Section II introduces our novel “Coupled CP Decomposition” (CCPD) and proposes an efficient algorithm for computing the CCPD solution; Section III further examines the theoretical properties of the CCPD via a simple, yet novel, analytical framework we expect may find use in other contexts; Section IV demonstrates the effectiveness of the CCPD in simulation; Section V then describes how the CCPD can be used to perform PCA on a set of undirected networks and Section VI demonstrates CCPD-based network PCA on two examples from political science and financial economics; finally Section VII concludes the paper and discusses several possible future directions for investigation.

Notation: Notation used in the paper follows that of Kolda and Bader [9] with a few minor modifications: we denote the general tensor-matrix product as \times_k and the (contractive) tensor-vector product as $\bar{\times}_k$. The tensor-vector product reduces the order of the product while the tensor-matrix product

M. Weylandt and G. Michailidis are both affiliated with the UF Informatics Institute at the University of Florida. G. Michailidis is also a Professor of Statistics and of Computer and Information Sciences at the University of Florida. (emails: michael.weylandt@ufl.edu and gmichail@ufl.edu)

maintains it: that is, if \mathcal{X} is a $2 \times 3 \times 4$ tensor and \mathbf{v} is a 4-vector or equivalently a 4×1 matrix, then $\mathcal{X} \times_3 \mathbf{v}$ is a $2 \times 3 \times 1$ tensor while $\mathcal{X} \bar{\times}_3 \mathbf{v}$ is a 2×3 matrix. While \circ denotes the general outer product, we also adopt the convention that when it is applied to two matrices of equivalent size, it denotes a matrix product with its transpose, not a higher order product: that is, if $\mathbf{V} \in \mathbb{R}^{p \times k}$, $\mathbf{V} \circ \mathbf{V} = \mathbf{V}\mathbf{V}^T$, a $p \times p$ matrix, not a $p \times k \times p \times k$ tensor. For a $p \times p \times T$ semi-symmetric tensor \mathcal{X} and a $p \times k$ matrix \mathbf{V} , we define the trace-product $[\mathcal{X}; \mathbf{V}]$ as the T -vector whose j^{th} element is given by $\langle \mathcal{X}_{\cdot, j}, \mathbf{V}\mathbf{V}^T \rangle = \text{Tr}(\mathbf{V}^T \mathcal{X}_{\cdot, j} \mathbf{V})$. Unless otherwise noted, inner products and norms refer to the Frobenius norm and associated inner product ($\|\mathcal{X}\| = \|\text{vec}(\mathcal{X})\|_{\ell_2}$ and $\langle \mathcal{X}, \mathcal{Y} \rangle = \sum_i \text{vec}(\mathcal{X})_i \text{vec}(\mathcal{Y})_i$). We denote the (compact) Stiefel manifold by $\mathcal{V}^{p \times r} = \{\mathbf{V} \in \mathbb{R}^{p \times r} : \mathbf{V}^T \mathbf{V} = \mathbf{I}_{r \times r}\}$. Finally, the matrix operator norm $\|\cdot\|_{\text{op}}$ is given by the absolute value of the largest magnitude eigenvalue for symmetric matrices and by $\|\mathcal{X}\|_{r\text{-op}} = \max_{\mathbf{u}, \mathbf{v} \in \mathbb{B}^T \times \mathcal{V}^{p \times r}} |\langle [\mathcal{X}; \mathbf{V}], \mathbf{u} \rangle|$ for semi-symmetric tensors, where \mathbb{B}^T is the unit ball in \mathbb{R}^T . In general, computing the semi-symmetric operator norm is difficult to compute, but Proposition 2 in Section III gives a tractable upper bound in terms of the operator norm of the slices of \mathcal{X} .

II. THE COUPLED CP DECOMPOSITION

The goal is to develop a tensor PCA framework which is able to capture realistic network structures in its output. While real-world networks have a variety of structures, we focus here on networks which are (approximately) low-rank, as these are most well-suited for PCA-type analyses. Many network models are approximately low-rank (in expectation), most notably, the random dot-product graph family [13], which includes both latent position and stochastic block models as special cases. These models have found use in a wide range of contexts, including analysis of social media networks, brain connectivity networks, and genomic networks [14], [15].

With these low-rank models in mind, we introduce our ‘‘Coupled CP Decomposition’’ (CCPD), which approximates a $p \times p \times T$ semi-symmetric tensor \mathcal{X} by a rank- r ‘‘principal component’’ and a loading vector for the final mode, which we typically take to represent independent replicates observed over time. As seen in the sequel, it is natural in many applications to interpret these as a ‘‘principal network’’ and a ‘‘time factor,’’ but this viewpoint is not essential for the technical developments of this section.

The single-factor rank- r CCPD is defined by

$$\mathcal{X} \approx d \mathbf{V} \circ \mathbf{V}^T \circ \mathbf{u}$$

where $\mathbf{u} \in \mathbb{R}^T$ is a unit-norm T -vector, $d \in \mathbb{R}_{\geq 0}$ is a scale factor, and $\mathbf{V} \in \mathcal{V}^{p \times r}$ is an orthogonal matrix satisfying $\mathbf{V}^T \mathbf{V} = \mathbf{I}_{r \times r}$. The name ‘‘coupled’’ comes from viewing this model as a CP-type decomposition

$$\mathcal{X} \approx \sum_{i=1}^r \lambda_i \mathbf{a}_i \circ \mathbf{b}_i \circ \mathbf{c}_i$$

where we require $\mathbf{a}_i = \mathbf{b}_i$ and $\mathbf{c}_i = \mathbf{c}_1$ for all $1 \leq i \leq r$ as well as $\langle \mathbf{a}_i, \mathbf{a}_j \rangle = \delta_{ij}$ to ensure orthogonality. This ‘‘coupling’’

restricts the number of parameters from $r(2p + T + 1) + pr + T - r(r + 1)/2 + 1$, which significantly improves both computational performance and estimation accuracy, as will be described in more detail below.

A more general CCPD, which we denote as the (r_1, \dots, r_K) -CCPD, may be defined by

$$\mathcal{X} \approx \sum_{k=1}^K d_k \mathbf{V}_k \circ \mathbf{V}_k \circ \mathbf{u}_k,$$

where, as before, each \mathbf{u}_k is a unit-norm T -vector, d_k are positive scale factors, and $\mathbf{V}_k \in \mathcal{V}^{p \times r_k}$ are orthogonal matrices used to construct the low-rank principal networks. Unless otherwise stated, we focus on the single-factor CCPD in our theory and experiments below, but extensions to the general case are straight-forward.

To compute the CCPD, we seek the best approximation in the Frobenius norm:

$$\begin{aligned} & \arg \min_{\mathbf{u}, \mathbf{V}, d} \|\mathcal{X} - d \mathbf{V} \circ \mathbf{V} \circ \mathbf{u}\|_F^2 \\ & \text{subject to } \mathbf{u} \in \mathbb{R}^T, \|\mathbf{u}\| = 1 \\ & \quad d \in \mathbb{R}_{\geq 0} \\ & \quad \mathbf{V} \in \mathcal{V}^{p \times r} \end{aligned}$$

It is easily seen that solving this problem is equivalent to minimizing the inner product:

$$\langle \mathcal{X}, \mathbf{V} \circ \mathbf{V} \circ \mathbf{u} \rangle = \langle \mathcal{X} \bar{\times}_3 \mathbf{u}, \mathbf{V} \circ \mathbf{V} \rangle$$

While this problem is difficult to optimize jointly in \mathbf{u} and \mathbf{V} , global solutions are available in closed form for \mathbf{u} with \mathbf{V} held constant and for \mathbf{V} with \mathbf{u} held constant. This motivates an alternating minimization (block coordinate descent) strategy comprised of alternating \mathbf{u} and \mathbf{V} updates. Specifically, holding \mathbf{u} constant, the optimal value of \mathbf{V} is simply the principal r eigenvalues of $\mathcal{X} \bar{\times}_3 \mathbf{u}$ and, holding \mathbf{V} constant, the optimal value of \mathbf{u} is a unit vector in the direction of $[\mathcal{X}; \mathbf{V}]$. Note that, for the single factor rank-1 CCPD, the \mathbf{V} -update simplifies to $\mathbf{u} \propto \mathcal{X} \bar{\times}_1 \mathbf{v} \bar{\times}_2 \mathbf{v}$. Putting these steps together, our single-factor rank- r CCPD algorithm is given by the following Algorithm:

Algorithm 1 Alternating Minimization Algorithm for the Rank- r Single-Factor CCPD

- Input: $\mathbf{u}^{(0)}$
 - Initialize: $k = 0$
 - Repeat until convergence:
 - (i) $\mathbf{V}^{(k+1)} = r\text{-eigen}(\mathcal{X} \bar{\times}_3 \mathbf{u}^{(k)})$
 - (ii) $\mathbf{u}^{(k+1)} = \text{Norm}([\mathcal{X}; \mathbf{V}^{(k+1)}])$
 - (iii) $k := k + 1$
 - Return $\hat{\mathbf{u}} = \mathbf{u}^{(k)}$, $\hat{\mathbf{V}} = \mathbf{V}^{(k)}$, $d = \langle \mathcal{X}, \hat{\mathbf{V}} \circ \hat{\mathbf{V}} \circ \hat{\mathbf{u}} \rangle_F$, and $\hat{\mathcal{X}} = d \hat{\mathbf{V}} \circ \hat{\mathbf{V}} \circ \hat{\mathbf{u}}$.
-

where $\text{Norm}(x) = x/\|x\|$ and $r\text{-eigen}(\mathbf{X})$ denotes the first r eigenvectors of \mathbf{X} . When \mathbf{X} has both positive and negative eigenvalues, $r\text{-eigen}(\mathbf{X})$ denotes those eigenvectors whose eigenvalues have the largest magnitudes. Convergence of Algorithm 1 follows from a minor extension of the results

of Regalia and Kofidis [16], [17], noting that the use of an eigendecomposition allows the \mathbf{V} -update to be solved to global optimality.

Algorithm 1 can be straightforwardly extended to the case of the (r_1, \dots, r_K) -CCPD using a successive deflation (greedy) approach. As noted by Mackey [18], improved performance can be achieved by using a ‘‘projection deflation’’ technique rather than simply subtracting off the estimated factors. Extending this technique to the general CCPD, we obtain Algorithm 2:

Algorithm 2 Successive Deflation Algorithm for Multi-Factor (r_1, \dots, r_K) -CCPD

- Initialize: $\mathcal{X}^1 = \mathcal{X}$
 - For $k = 1, \dots, K$:
 - (i) Run Algorithm 1 on \mathcal{X}^k for rank r_k to obtain $(\mathbf{u}_k, \mathbf{V}_k, d_k)$
 - (ii) Deflate: $\mathcal{X}^{k+1} = \mathcal{X}^k \times_1 [\mathbf{I}_{p \times p} - \mathbf{V}_k \circ \mathbf{V}_k] \times_2 [\mathbf{I}_{p \times p} - \mathbf{V}_k \circ \mathbf{V}_k] \times_3 [\mathbf{I}_{T \times T} - \mathbf{u}_k \mathbf{u}_k^T]$
 - Return $\{\mathbf{u}_k\}, \{\mathbf{V}_k\}, \{d_k\}$
-

Algorithm 2 guarantees what Weylandt [19] terms ‘‘one-way orthogonality’’ at each step: that is, at each step, the target tensor \mathcal{X}^t satisfies the following:

$$\begin{aligned} \mathcal{X}^t \times_1 \mathbf{V}_t \circ \mathbf{V}_t &= \mathbf{0} \\ \mathcal{X}^t \times_2 \mathbf{V}_t \circ \mathbf{V}_t &= \mathbf{0} \\ \mathcal{X}^t \bar{\times}_3 \mathbf{u}_t &= \mathbf{0} \end{aligned}$$

By contrast, a standard deflation step, *i.e.*, $\mathcal{X}^t = \mathcal{X}^{t-1} - d_t \mathbf{V}_t \circ \mathbf{V}_t \circ \mathbf{u}_t$, only guarantees the weaker total orthogonality condition $\langle \mathcal{X}^t, \mathbf{V}_t \circ \mathbf{V}_t \circ \mathbf{u}_t \rangle = 0$. For a stronger form of orthogonality, we can use the deflation:

$$\mathcal{X}^{k+1} = \mathcal{X}^{\tilde{k}+1} \times_3 [\mathbf{I}_{T \times T} - \mathbf{u}_k \mathbf{u}_k^T]$$

where $\mathcal{X}^{\tilde{k}+1}$ is the tensor obtained by performing Schur complement deflation on each slice independently:

$$\mathcal{X}^{\tilde{k}+1} \dots_i = \mathcal{X}^k \dots_i - \mathcal{X}^k \dots_i \mathbf{V}_k (\mathbf{V}_k^T \mathcal{X}^k \dots_i \mathbf{V}_k)^{-1} \mathbf{V}_k^T \mathcal{X}^k \dots_i$$

for $1 \leq i \leq T$. This stronger deflation guarantees that

$$\begin{aligned} \mathcal{X}^{t+s} \times_1 \mathbf{V}_t \circ \mathbf{V}_t &= \mathbf{0} \quad \text{for } s \geq 0 \\ \mathcal{X}^{t+s} \times_2 \mathbf{V}_t \circ \mathbf{V}_t &= \mathbf{0} \quad \text{for } s \geq 0 \\ \mathcal{X}^t \bar{\times}_3 \mathbf{u}_t &= \mathbf{0} \end{aligned}$$

Proofs of these facts are simple extensions of those in Appendix A.2 of Weylandt [19].

As presented above, the runtime of Algorithm 1 is dominated by the tensor matrix multiplications $\mathcal{X} \bar{\times}_3 \mathbf{u}^{(k)}$ and $[\mathcal{X}, \mathbf{V}^{(k+1)}]$, with complexity $\mathcal{O}(Tp^2)$ and $\mathcal{O}(Tkp^2)$, respectively, as well as the eigendecomposition in the \mathbf{V} -update with complexity $\mathcal{O}(p^3)$. Together these yield an overall per iteration complexity of $\mathcal{O}(p^3 + Tkp^2)$ in a naïve implementation. While this is sufficient for moderate-scale data, these terms may scale poorly for very large-scale networks. We note however that the tensor multiplication steps are well-suited for parallel computation on modern general purpose GPUs and that randomized or iterative algorithms can be used to

reduce the cost of the eigendecomposition to $\mathcal{O}(k^2p)$ since only the leading k eigenvectors are required [20]–[22]; these algorithms exhibit particularly good performance for sparse tensors, the latter commonly arising in network data. If C cores are available to parallelize the tensor multiplication steps, the per iteration complexity can thus be reduced to $\mathcal{O}(k^2p + Tkp^2/C)$. The total complexity of Algorithm 1 will of course depend on the total number of iterations required: this quantity is difficult to give explicit estimates of, but as we will discuss in the next section, convergence to an estimate ‘‘within the noise’’ of the problem is typically quite fast under weak assumptions.

III. THEORETICAL PROPERTIES OF THE CCPD

Next, we investigate the theoretical properties of the CCPD and give a consistency result tailored for the Network PCA approach studied in the next section. Specifically, we consider a semi-symmetric tensor analogue of the ‘‘low-rank + noise’’ model often used to study matrix PCA:

$$\mathcal{X} = d \mathbf{V}_* \circ \mathbf{V}_* \circ \mathbf{u}_* + \mathcal{E} \quad (1)$$

where \mathbf{u}_* is a unit-norm T -vector, \mathbf{V}_* is a $p \times r$ orthogonal matrix satisfying $\mathbf{V}_*^T \mathbf{V}_* = \mathbf{I}_{r \times r}$, $d \in \mathbb{R}_{>0}$ is a measure of signal strength, and \mathcal{E} is a semi-symmetric noise tensor. This model generalizes the matrix case, with d playing the role of the leading singular value and $\mathbf{V}_*, \mathbf{u}_*$ being analogous to the singular vectors. To highlight the broad applicability of the CCPD, we give a general result based on a signal corrupted by sub-Gaussian noise in \mathcal{E} : in certain network applications, the noise model can be further restricted to 0/1 Bernoulli noise without significant difficulty. Under these assumptions, we have the following consistency result:

Theorem 1. *Suppose \mathcal{X} is generated from the semi-symmetric model described above (1) with elements of \mathcal{E} each independently σ^2 -sub-Gaussian, subject to symmetry constraints. Suppose further that the initialization \mathbf{u}_0 satisfies*

$$|1 - \langle \mathbf{u}_0, \mathbf{u}_* \rangle| \leq \tan^{-1}(0.5) - \frac{5 \|\mathcal{E}\|_{r-op}}{d(1-c)}$$

for some arbitrary $c < 1$. Then, the output of Algorithm 1 applied to \mathcal{X} satisfies the following

$$\min_{\mathbf{O} \in \mathcal{V}^{r \times r}} \frac{\|\mathbf{V}^* - \hat{\mathbf{V}} \mathbf{O}\|_2}{\sqrt{pr}} \lesssim \frac{\sigma r \sqrt{T}}{d(1-c)}$$

with high probability and where \lesssim denotes an inequality holding up to a universal constant factor and a term scaling as $\sqrt{\log T}$.

A similar result holds for the \mathbf{u} -factor:

Theorem 2. *Under the same conditions as Theorem 1, the output of Algorithm 1 applied to \mathcal{X} satisfies*

$$\min_{\epsilon = \pm 1} \|\epsilon \mathbf{u}_* - \hat{\mathbf{u}}\| / \sqrt{T} \lesssim \frac{\sigma r \sqrt{p}}{d(1-c)}$$

with high probability and \lesssim is as before.

We outline the proof of these results at the end of this section.

We note that a careful reading of the proofs of Theorems 1 and 2 also gives insights into the qualitative convergence behavior of Algorithm 1. Specifically, the proof establishes that the error after k iterations is of the form:

$$\text{Error in } \mathbf{u}_k \approx c^k E_1 + E_2 / (1 - c)$$

where E_1 is a term depending on the accuracy of the initialization \mathbf{u}_0 and E_2 is a term depending on the noise term \mathcal{E} and the signal strength d . For $c < 1$, this implies a two-phase convergence analysis: in early iterations, artifacts of initialization error (E_1) decay quickly (geometrically) until the irreducible statistical noise (E_2) dominates. This qualitative finding is consistent with our experimental results and mirrors similar findings in the sparse regression context [23]. This is a substantially different finding than a classical convergence rate for an iterative algorithm: we show here that the *statistical* quality of the iterates, *i.e.*, the difference between \mathbf{u}_k and \mathbf{u}_* , converges quickly to a (non-zero) amount, while classical analysis of this problem would consider convergence of the difference between \mathbf{u}_k and $\hat{\mathbf{u}} = \mathbf{u}_\infty$ to zero.

It is instructive to compare Theorems 1 and 2 to similar results for the matrix SVD: specifically, under the matrix model

$$\mathbf{X} = d \mathbf{u}_* \mathbf{v}_* + \mathbf{E} \in \mathbb{R}^{T \times p}$$

where elements of \mathbf{E} are independently σ^2 -sub-Gaussian a Davis-Kahan-type analysis [24, Theorem 3] yields:

$$\begin{aligned} \min_{\epsilon \in \pm 1} \|\hat{\mathbf{v}}_\epsilon - \mathbf{v}_*\| &\leq \frac{2^{3/2} \|\mathbf{E}\|_{\text{op}}}{d} \\ &\lesssim \frac{\sigma \sqrt{T+p}}{d} \\ \implies \min_{\epsilon \in \pm 1} \|\hat{\mathbf{v}}_\epsilon - \mathbf{v}_*\| / \sqrt{p} &\lesssim \sigma \sqrt{T} / d. \end{aligned}$$

where “ \lesssim ” denotes an upper bound holding up to a universal constant with high probability. Similarly, analyzing the right singular vector, we find

$$\min_{\epsilon \in \pm 1} \|\hat{\mathbf{u}}_\epsilon - \mathbf{u}_*\| / \sqrt{T} \lesssim \sigma \sqrt{p} / d$$

We see here that for both the matrix and the tensor model, the error in the estimated factors behaves as σ/d times the square root of the other dimension. Furthermore, we can compare the reconstruction error of our two models: the normalized reconstruction error of matrix PCA is given by

$$\text{Error}(\hat{\mathbf{u}} \hat{\mathbf{v}}^T, \mathbf{u}_* \mathbf{v}_*) \lesssim \left(\frac{\sigma \sqrt{T}}{d} \right) \left(\frac{\sigma \sqrt{p}}{d} \right) = \frac{\sigma^2}{d^2} \sqrt{Tp}$$

The normalized reconstruction error of the CCPD is given by

$$\begin{aligned} &\text{Error}(\hat{\mathbf{v}} \circ \hat{\mathbf{v}} \circ \hat{\mathbf{u}}, \mathbf{v}_* \circ \mathbf{v}_* \circ \mathbf{u}_*) \\ &\leq \|\hat{\mathbf{v}} \circ \hat{\mathbf{v}} - \mathbf{v}_* \circ \mathbf{v}_*\| \|\hat{\mathbf{u}} - \mathbf{u}_*\| \\ &\lesssim \|\hat{\mathbf{v}} - \mathbf{v}_*\| \|\hat{\mathbf{v}} + \mathbf{v}_*\| \|\hat{\mathbf{u}} - \mathbf{u}_*\| \\ &\lesssim \|\hat{\mathbf{v}} - \mathbf{v}_*\| \|\hat{\mathbf{u}} - \mathbf{u}_*\| \\ &\lesssim \left(\frac{\sigma \sqrt{p}}{d} \right) \left(\frac{\sigma \sqrt{T}}{d} \right) = \frac{\sigma^2}{d^2} \sqrt{Tp} \end{aligned}$$

which is the same rate as matrix PCA. Note that we avoid

squaring the estimation error in the \mathbf{V} -factor by noting that $\|\hat{\mathbf{v}} + \mathbf{v}_*\|$ is bounded above by a universal constant since all terms are unit vectors.

These comparisons suggest that our CCPD, and Network PCA methods based upon it, will exhibit similar statistical performance as widely-used matrix PCA and that it provides a natural starting point for analyzing network series data. The tensor setting does not have the elegant spectral properties of matrix eigendecomposition and requires moderately stringent conditions on the initial guess \mathbf{u}_0 . As we argue next, these initialization conditions are often quite naturally satisfied and our approach can obtain good results even with random initialization.

A. Stable Initialization

Theorems 1 and 2 hold under quite general conditions, but the reader may be concerned about the difficulty in verifying the initialization condition on \mathbf{u}_0 : in the noiseless case ($\|\mathcal{E}\|_{r\text{-op}} = 0$), the initialization condition holds as long as the angle between \mathbf{u}_0 and \mathbf{u}_* is less than approximately 57.3° , with a tighter initialization required in the noisy case. In low- to moderate-dimensional settings, this condition may be expected to hold under random initialization, but in high-dimensional settings, it is unlikely to hold. To address this, we introduce the following *stability* condition on \mathbf{u}_* :

Proposition 1. *Suppose \mathbf{u}_* is a δ -stable unit vector in \mathbb{R}^T , in the sense that*

$$|\langle \mathbf{u}_*, \mathbf{1}_T / \sqrt{T} \rangle - 1| \leq \delta,$$

where $\mathbf{1}_T$ is the all-ones vector in \mathbb{R}^T for

$$\delta \leq \tan^{-1}(0.5) - \frac{5\sigma \sqrt{p}}{d(1-c)}$$

Then, the initialization condition of Theorems 1 and 2 holds with high probability when Algorithm 1 is initialized at $\mathbf{u}_0 = \mathbf{1}_T / \sqrt{T}$.

The above stability condition implies that \mathbf{u}_* is “approximately constant” and that the (scaled) all-ones vector provides a good initialization to Algorithm 1. We expect this assumption to be a reasonable one in most applications: *e.g.*, if \mathcal{X} represents correlation of financial assets or linkages in a social network over multiple time periods, we expect the main signal to remain roughly constant over time. It would be highly unusual for correlated financial instruments to suddenly become anti-correlated or for all connections in a social network to vanish and be replaced at random. While the stability condition may be expected to hold in many scenarios and to give guidance for initializing Algorithm 1, we have found that random initialization also performs quite well in practice, as shown by the numerical results in the next section.

By analogy with the stability condition, we refer to the choice of $\mathbf{u}_0 = \mathbf{1}_T / \sqrt{T}$ as “stable initialization” for Algorithm 1. Stable initialization admits a particularly nice interpretation of the first \mathbf{V} -update in Algorithm 2 which we highlight below:

Remark 1. Under the stable initialization condition $\mathbf{u}_0 = \mathbf{1}_T/\sqrt{T}$ and the low-rank + noise model assumed in Theorems 1 and 2, the first step of Algorithm 1 implicitly estimates $\mathbf{V}_* \circ \mathbf{V}_*$ via the sample average of T observations; specifically,

$$d\mathbf{V}_* \circ \mathbf{V}_* \approx d\mathbf{V}_* \circ \mathbf{V}_* \langle \mathbf{u}_0, \mathbf{u}_* \rangle + \mathcal{E} \bar{\times}_3 \mathbf{u}_0$$

For large values of $\langle \mathbf{u}_0, \mathbf{u}_* \rangle$, the first term dominates the second, implying an effective initialization. Specifically, the stable-initialization condition implies

$$\|\sin \Theta(\mathbf{V}^*, \mathbf{V}^{(1)})\|_F \leq \frac{2r^{1/2} \|\tilde{\mathbf{E}}\|_{op}}{d \langle \mathbf{u}_*, \mathbf{u}_0 \rangle}$$

where $\tilde{\mathbf{E}} = \mathcal{E} \bar{\times}_3 \mathbf{u}_0$ is a symmetric matrix with independently σ^2 -sub-Gaussian elements, and hence $\|\tilde{\mathbf{E}}\|_{op}$ is of the order $\sigma\sqrt{p}$ with high probability.

Of course, the variance of this initial estimator could be improved by knowing the ‘‘oracle’’ initialization $\mathbf{u}_0 = \mathbf{u}_*$, but even this simple initialization scheme works well in practice. This heuristic analysis can also be extended to the case of random initialization by noting that $\langle \mathbf{u}_*, \mathbf{u}_0 \rangle$ is unlikely to be exactly zero by chance and so some signal is likely to persist in the initial \mathbf{V} -update by chance. When d is sufficiently large, this residual signal can be expected to dwarf the noise term and Algorithm 1 will again be well initialized.

We note here that we focus on the case where neither \mathbf{u}_* or \mathbf{V}_* are assumed sparse. This limits our theoretical results to the low-dimensional regime ($T \propto p^2$ rather than $T \propto \log p$), but we feel these are most useful for the network applications described in later sections. Specifically, if we consider the rank-1 CCPD, zero elements of \mathbf{V}_* correspond to isolated nodes in the network $\mathbf{V}_* \circ \mathbf{V}_*$, which are more naturally omitted from the construction of the data tensor rather than included in PCA-type analyses. Our approach could be straight-forwardly extended to the high-dimensional regime by replacing the \mathbf{V} -update with one or more iterations of sparse eigenvalue estimator such as the truncated power method [25]. Alternatively, if we assume a minimum edge strength, our results can be extended to the high-dimensional case by adding a truncation step at the end of Algorithm 1 in a manner similar to recent analyses of the high-dimensional regression problem [26]

B. Key Steps in Establishing the Theoretical Results

The key steps and corresponding techniques used in the proofs of our theoretical results may be of independent interest; hence, we briefly describe them next and give the full proof in the supplementary materials found at the end of this paper.

Our proof consists of bounding the error at iteration $k+1$ as a sum of two terms: the first depending on the error at iteration k and the second depending on the noise tensor through its operator norm $\|\mathcal{E}\|_{r\text{-op}}$. The treatment of the noise tensor is similar to modern analysis of the (matrix) power method under noise [27], thus, we do not dwell on it here. Our major technical tool for obtaining the first term of the error bound

is the Davis-Kahan theorem [28], specifically in the form given by Yu, Wang, and Samworth [24]. Expanding $\mathcal{X} \bar{\times}_3 \mathbf{u}^{(k)}$ under our model for \mathcal{X} , we can use the Davis-Kahan result applied to the pair $\Sigma^* = d\mathbf{v}_* \circ \mathbf{v}_*$ and $\tilde{\Sigma} = \mathcal{X} \bar{\times}_3 \mathbf{u}^{(k)}$ to get a bound relating the error in $\mathbf{v}^{(k+1)}$ to the error in $\mathbf{u}^{(k)}$. The non-linear normalization step in the \mathbf{u} -update makes it more difficult to employ the Davis-Kahan result a second time, but this can be circumvented by applying the theorem to $[\mathcal{X}, \mathbf{V}^{(k+1)}] \circ [\mathcal{X}, \mathbf{V}^{(k+1)}]$ and $d^2 \mathbf{u}_* \circ \mathbf{u}_*$, the latter of which has a good eigenvector by construction, to get a bound on the error of $\mathbf{u}^{(k)}$ in terms of $\mathbf{v}^{(k)}$. Subsequently, a careful recursive application of these bounds gives the results stated above as the number of iterations k goes to infinity.

The key to applying the recursive bounds is ensuring that we have a contraction at each step. While this is simple in the noiseless case, and implies eventual convergence to the true solution, it is more challenging in the noisy case. To handle this, we consider a ‘‘noisy contraction’’ model, where we contract towards the true parameter, but then add back a noise term. The ratio of the contraction rate and the noise term gives the error of the final solution; in our case, this works out to $\|\mathcal{E}\|_{r\text{-op}}/(1-c)$ where $c < 1$ is an arbitrary constant depending on the quality of the initialization. This noisy contraction framework has appeared in previous work on sparse regression [23] and we expect it to prove useful in analyzing other algorithmically-defined estimators for non-convex problems. The theoretical results of Sun, Lu, Liu, et al. [29] are most similar to ours, though their analysis requires more restrictive assumptions and a far more technical analysis than we employ here.

Finally, we use the following result, with proof in the Supplementary Materials, to control $\|\mathcal{E}\|_{r\text{-op}}$:

Proposition 2. *The semi-symmetric operator norm, $\|\mathcal{X}\|_{r\text{-op}} = \max_{\mathbf{u}, \mathbf{V} \in \mathbb{B}^T \times \mathcal{V}^p \times \mathcal{V}^r} |[\mathcal{X}, \mathbf{V}]^T \mathbf{u}|$ can be bounded above by $r\sqrt{T} \max_i \lambda_{\max}(\mathcal{X}_{..i})$. Furthermore, if the elements of \mathcal{X} are independently σ^2 -sub-Gaussian, subject to symmetry constraints, we have*

$$\|\mathcal{X}\|_{r\text{-op}} \leq cr\sqrt{T}\sigma \left(\sqrt{p} + \sqrt{\log T} + \delta \right)$$

with probability at least $1 - 4e^{-\delta^2}$, for some absolute constant c .

The claim in Remark 1 can be established by noting that

$$\begin{aligned} \mathbf{V}^{(1)} &= \text{eigen}(\mathcal{X} \bar{\times}_3 \mathbf{u}_0) \\ &= \text{eigen} \left(\underbrace{d\mathbf{V}_* \circ \mathbf{V}_* \langle \mathbf{u}_*, \mathbf{u}_0 \rangle}_{\text{Signal} = \tilde{\mathbf{A}}} + \underbrace{\mathcal{E} \bar{\times}_3 \mathbf{u}_0}_{\text{Noise} = \tilde{\mathbf{E}}} \right) \end{aligned}$$

where the signal term $\tilde{\mathbf{A}}$ has non-zero eigenvalues all at least $d \langle \mathbf{u}_*, \mathbf{u}_0 \rangle$ and the noise term $\tilde{\mathbf{E}}$ is a symmetric matrix whose elements are independently σ^2 -sub-Gaussian. Applying the Davis-Kahan theorem yields Remark 1

IV. NUMERICAL EXPERIMENTS

Next, we demonstrate the effective performance of the CCPD model at recovering both the ‘‘time factor’’ \mathbf{u}_* and

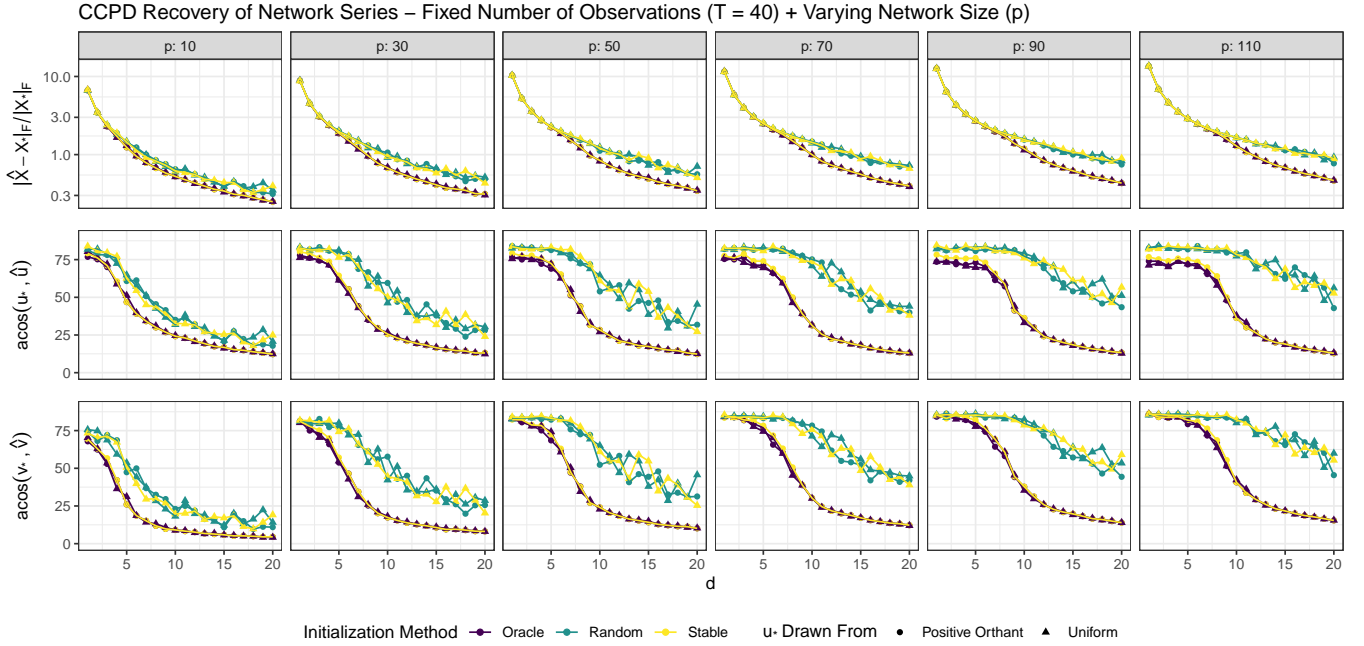


Fig. 1: Performance of Algorithm 1 for recovery of a rank-1 semi-symmetric tensor of norm d with added noise from a Gaussian Orthogonal Ensemble. Tensor recovery is accurate across several measures including the normalized reconstruction error between $\hat{\mathcal{X}}$ from Algorithm 1 and the signal tensor $\mathcal{X}_* = d\mathbf{V}_* \circ \mathbf{V}_* \circ \mathbf{u}_*$ (top row), the angle between \mathbf{u}_* and $\hat{\mathbf{u}}$ (middle row), and the angle between \mathbf{V}_* and $\hat{\mathbf{V}}$ (bottom row). As expected, oracle initialization (purple, $\mathbf{u}_0 = \mathbf{u}_*$) consistently performs the best of the initialization schemes considered, but random initialization (green) and “stable” initialization (yellow, to the all-ones vector) also perform well. In scenarios where \mathbf{u}_* is restricted to have all positive elements, stable initialization performs almost indistinguishably from oracle initialization; in scenarios where \mathbf{u}_* is allowed to have both positive and negative elements, stable initialization performs essentially as well as random initialization, suggesting that our method is quite robust to the specific choice of initialization. We fix $T = 40$ observations and vary the dimension of \mathbf{V}_* from 10 (far left column) to 110 (far right column); as would be expected, performance does decay for larger dimensions, but the decay is rather slow, consistent with our theoretical results.

the “base network” \mathbf{V}_* . To do so, we apply Algorithm 1 to \mathcal{X} generated from the model $\mathcal{X} = d\mathbf{V}_* \circ \mathbf{V}_* \circ \mathbf{u}_* + \mathcal{E}$, with $r = 1$. Because our main theorems do not place any restrictions on \mathbf{V}_* , we draw \mathbf{V}_* uniformly at random from the rank-1 Stiefel manifold (unit sphere). To investigate the relevance of the δ -stability assumption on \mathbf{u}_* , we consider two cases with \mathbf{u}_* drawn uniformly at random from the unit sphere and from \mathbf{u}_* drawn uniformly from the positive orthant of the unit sphere, *i.e.*, unit vectors with all positive elements. Finally, we generate \mathcal{E} such that each slice of \mathcal{E} is an independent draw from the Gaussian orthogonal ensemble (GOE): that is, the off-diagonal elements are drawn from independent standard normal distributions and the diagonal elements are independent samples from a $\mathcal{N}(0, 2)$ distribution. From well-known bounds on the GOE, we have $\|\mathcal{E}\|_{\text{op}} \approx \sqrt{pT}$, giving an effective signal-to-noise ratio of d/\sqrt{pT} for all experiments. Finally, we investigate the effect of the \mathbf{u}_0 initialization by considering three initialization schemes: i) an “Oracle” initialization scheme, where $\mathbf{u}_0 = \mathbf{u}_*$; ii) a purely random initialization scheme where \mathbf{u}_0 is drawn at random from the unit sphere; and iii) a “stable” initialization scheme corresponding to Proposition 1 with $\mathbf{u}_0 = \mathbf{1}_T/\sqrt{T}$.

Figure 1 shows the results of our study in the case of

fixed T (number of samples) and varying p (network size) from 10 to 110. We present three measures of accuracy: the normalized reconstruction error between $\hat{\mathcal{X}} = \hat{d}\hat{\mathbf{V}} \circ \hat{\mathbf{V}} \circ \hat{\mathbf{u}}$ and the signal tensor $\mathcal{X}_* = d\mathbf{V}_* \circ \mathbf{V}_* \circ \mathbf{u}_*$; the angle between \mathbf{u}_* and $\hat{\mathbf{u}}$, and the angle between the subspaces spanned by \mathbf{V}_* and $\hat{\mathbf{V}}$, calculated as $\cos^{-1}[\sigma_{\min}(\mathbf{V}_*^T \hat{\mathbf{V}})]$, where $\sigma_{\min}(\cdot)$ denotes the last (non-zero) singular value. Consistent with Theorems 1 and 2, we observe errors that decay rapidly in d for all three measures under all generative and initialization schemes. Comparing the case with \mathbf{u}_* from the positive orthant or the entire unit sphere, we observe that random initialization does well in both cases, with accuracy only slightly worse than oracle initialization, and that stable initialization achieves essentially the same performance as oracle initialization for positive \mathbf{u}_* .

Figure 2 presents similar results taking the network size of $p = 40$ nodes fixed and varying T , though here with the effective signal-to-noise ratio d/\sqrt{pT} on the ordinate (x -axis) rather than the scale factor d . As in Figure 1, the results of Theorems 1 and 2 are confirmed, with error decaying quickly and accurate recovery even at signal-to-noise ratios of approximately 1, and with both random and stable initial-

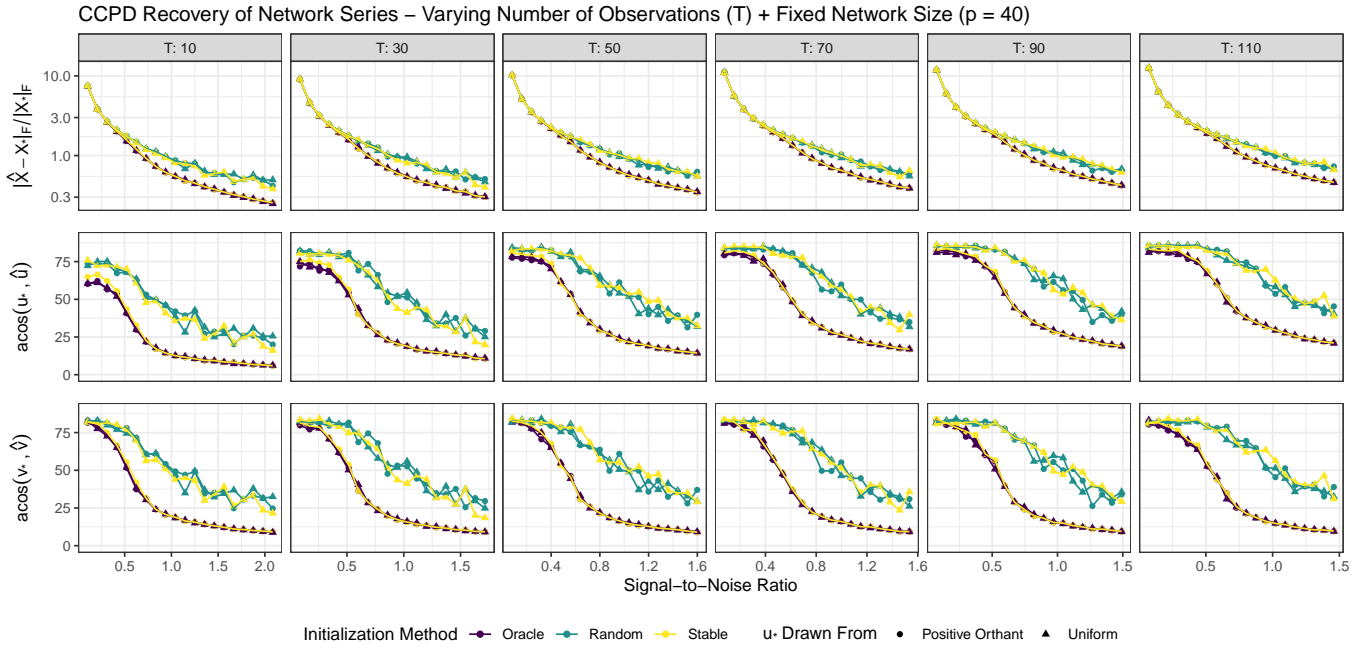


Fig. 2: Performance of Algorithm 1 for recovery of a rank-1 semi-symmetric tensor of norm d with added noise from a Gaussian Orthogonal Ensemble. Under the same generative model as Figure 1, we here fix the dimension of \mathbf{V}_* at 40 and vary the number of observations T from $T = 10$ (far left) to $T = 110$ (far right). Here we rescale the x -axis to the effective signal-to-noise ratio $d/(\sqrt{pT})$ and note that accuracy to within 25° can be obtained even in relatively difficult SNR ≈ 1 scenarios. (For $p = 40$, $\angle(\hat{\mathbf{V}}, \mathbf{V}_*) \approx 25^\circ$ corresponds to an ℓ_2 error of $\sqrt{2} \sin(25^\circ) \approx 0.6$ or a root mean squared error 0.1 across all elements of $\hat{\mathbf{V}}$. This is well within the bounds of usability for many network science applications where the elements of \mathcal{X} take $\{0, 1\}$ -values.

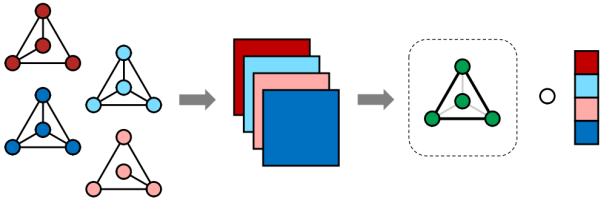


Fig. 3: Application of CCPD for Network PCA: Given a collection of networks (left panel), these can be encoded as symmetric matrices using, *e.g.*, adjacency matrix or graph Laplacian representations, and formed into a semi-symmetric tensor (center panel). Apply the CCPD to this semi-symmetric tensor yields a “principal network” ($\hat{\mathbf{V}} \circ \hat{\mathbf{V}}$, in green) and loading vector ($\hat{\mathbf{u}}$, rightmost element) which attempt to capture significant common patterns amongst the networks, *e.g.*, the “outer triangle” edges (right panel).

izations being qualitative competitive with the oracle one and with the stable initialization being essentially indistinguishable from the oracle one for positive \mathbf{u}_* . Taken together, these two experiments demonstrate that the CCPD model and Algorithm 1 are robust to the initialization scheme, perform well even in situations where the theoretical requirements of Theorems 1 and 2 are violated, and are well-suited for the range of applications we describe in the following two sections.

V. NETWORK PCA VIA THE CCPD MODEL

In this section, we demonstrate how the CCPD model can be used for performing principal components analysis on time series of networks. Specifically, we assume that we are given T observations of networks on the same p nodes with the node identities being known and held constant across observations, *i.e.*, no “label-switching” effects. These networks $\{\mathcal{G}_i\}_{i=1}^T$ can then each be represented in a matrix $\mathbf{X}_i \in \mathbb{R}^{p \times p}$ ($1 \leq i \leq T$) with the adjacency matrix and the (possibly normalized and degree-corrected / regularized) graph Laplacian representations being preferred in most applications [30]. Aligning these matrices as slices of a tensor $\mathcal{X} \in \mathbb{R}^{p \times p \times T}$ ($\mathcal{X}_{\cdot i} = \mathbf{X}_i$), we obtain a semi-symmetric tensor suitable for CCPD-decomposition. This process is illustrated in Figure 3. We focus on three main uses of PCA, roughly corresponding to first-moment (mean) analysis, second-moment (variance) analysis, and changepoint detection, but emphasize that our decomposition can be used wherever PCA is used, *e.g.*, spectral clustering or manifold learning.

A. Identifying Principal Networks

The first and most common use of the CCPD for Network PCA is in identifying “principal networks,” which we identify with the \mathbf{V}_k -factors produced by Algorithm 2. Specifically, the outer product of each \mathbf{V}_k factor with itself $\mathbf{V}_k \circ \mathbf{V}_k = \mathbf{V}_k \mathbf{V}_k^T$ can be interpreted as a $p \times p$ matrix capturing major patterns in

the data tensor \mathcal{X} . These principal networks play the same role as the eigenvectors or right singular vectors from traditional (eigendecomposition- or SVD-based) PCA for vector data, highlighting common structures across observations. These “principal networks” can also be used to construct low-dimensional representations for use in downstream analyses by computing $\langle \hat{\mathbf{X}}, \mathbf{V}_k \circ \mathbf{V}_k \rangle$ for each network \mathbf{V}_k and a new observation $\hat{\mathbf{X}}$ on the same node set. As discussed in Section III, each estimate $\hat{\mathbf{V}}$ can be interpreted as the leading eigenspace of the weighted matrix sum $\sum_{i=1}^T u_i \mathbf{X}_i$ with the weights u_i chosen to maximize informativeness of this sum. Because Algorithm 2 allows different time factors \mathbf{u} for each factor, our approach is able to identify multiple principal networks in data sets with complex structure.

As with matrix PCA, selection of the optimal ranks (r_1, \dots, r_K) for use in Algorithm 2 is a challenging problem for which a fully satisfactory answer is not readily available. Many heuristics have been proposed for rank selection in matrix PCA [31]–[34], typically based on decreasing explanatory power or a more general information criterion-based model selection framework. In our experiments, we have found that a greedy approach where each rank r_i is chosen by maximizing the BIC performs well [35], but tensor analogues of data-driven approaches for PCA have also been shown to perform well in similar settings [36]. Unlike matrix PCA, tensor decomposition methods are not based on ordered singular vectors and cannot guarantee nestedness or orderedness of the estimated factors *a priori*. In practice, we have found that the greedy structure of Algorithm 2, which combines a power method and a strict deflation step, produces well-ordered factors (decreasing values of $\{d_i\}$) and gives nestedness by construction. Similar behavior has been observed in other power method contexts, including differentially private PCA [27], sparse matrix PCA [37], and regularized tensor factorization [11], [12]. Because Algorithm 2 does not enforce orthogonality of the estimated components \mathbf{V}_i and \mathbf{V}_j as in matrix PCA, the specific choice of rank is less important than in matrix PCA, so long as the rank is as high as the rank of the target network, as has been recently noted for several other decomposition schemes, *e.g.*, non-negative matrix factorization [38].

B. Characterizing Modes of Variation

Beyond identifying principal networks, the CCPD model and associated Network PCA scheme is also useful for identifying patterns of typical deviation from those networks. Specifically, if we apply the CCPD to $\mathcal{X} - \hat{\mathcal{X}}$ with $\hat{\mathcal{X}}$ estimated via Algorithm 1, the estimated principal networks $\hat{\mathbf{V}} \circ \hat{\mathbf{V}}$ will capture the major modes of variation away from the baseline principal network. This is perhaps the application of Network PCA most similar to standard PCA, where the eigenvectors of the (centered) scatter matrix capture the second moment (variance) in the population.

As with matrix PCA, the observation loading vector \mathbf{u} is particularly useful for analyzing variability: disproportionately large values of u_i indicate “high-leverage” observations which significantly depart from the bulk of observations [39]. Specifically, we have found that examining the observations with the

highest values of $|u_i|$ serves as a useful heuristic for outlier-detection. Future work is needed to precisely determine the sampling behavior of \mathbf{u} and to make this heuristic rigorous for the tensor case.

C. Change point Detection in Network Time series Data

Finally, we note that Network PCA-type techniques can be used to identify change points in a time-ordered network series under a rank- r mean-shift model. Specifically, we adapt a proposal of Wang and Samworth [40] to the network setting and perform Network PCA on the Cumulative Sum Control Chart (“CUSUM”) tensor \mathcal{C} given by

$$\mathcal{C}_{ijt} = \sqrt{\frac{T}{t(T-t)}} \left(\frac{t}{T} \sum_{\tau=1}^t \mathcal{X}_{ij\tau} - \sum_{\tau=1}^T \mathcal{X}_{ij\tau} \right)$$

By construction, $\mathcal{C} \in \mathbb{R}^{p \times p \times (T-1)}$ inherits the semi-symmetric structure of \mathcal{X} and so can be used as input to Algorithm 1 with rank r . The resulting “time factor,” $\hat{\mathbf{u}}$, can then be used for change point analysis with $\hat{\tau} = \arg \max_{1 \leq \tau \leq (T-1)} |\hat{u}_\tau|$ being the most likely change point. A combination of Theorem 2 and standard change point detection theory implies that this approach correctly identifies a change point from data generated with mean $\mathbf{V}_*^{(1)}$ to $\mathbf{V}_*^{(2)}$ with probability inversely proportional to the effective signal-to-noise ratio

$$\left\| \mathbf{V}_*^{(1)} - \mathbf{V}_*^{(2)} \right\|_{\text{op}} \sqrt{\min\{\tau^{(1)}, \tau^{(2)}\}} / \sigma$$

where $\tau^{(1)}$ and $\tau^{(2)}$ are the number of observations before and after the change point directly. This compares well with optimal rates for the univariate CUSUM model [41] and with recent work on network change point detection [42], specializing the latter results to the low-dimensional (non-sparse) regime.

In the following section, we apply the three techniques leveraging the CCPD model described in this section to two example data sets drawn from political science and from quantitative finance.

VI. APPLICATION TO REAL-WORLD NETWORKS

A. Analysis of U.S. Supreme Court Voting Patterns

We next use the CCPD and associated Network PCA strategy to analyze the voting behavior of the Supreme Court of the United States (SCOTUS) from a period from 1995 to June 2021. Specifically, we construct a series of 9×9 networks with nodes corresponding to each “seat” on the court: that is, a justice and her successor are assigned to the same node even if they have substantially different judicial philosophies, *e.g.*, Ruth Bader Ginsberg and Amy Coney Barrett. Edge weights for each network are given by the fraction of cases in which the pair of justices agree in the specific judgement of the court: we ignore additional subtleties that arise when two justices agree on the outcome, but disagree on the legal reasoning used to reach that conclusion. We repeat this process for 25 year-long terms beginning in October 1995 (“October Term 1995” or “OT 1995”) to the term ending in June 2021 (“OT 2020”). Our results are presented in Figure 4.

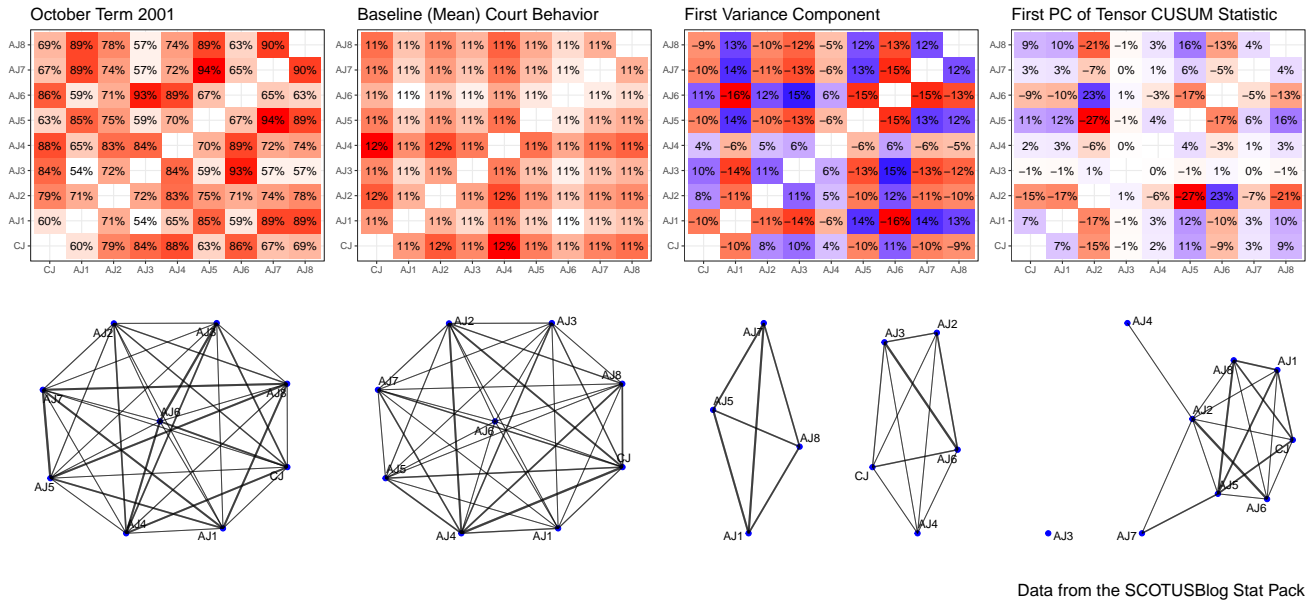


Fig. 4: Application of the CCPD model to the Supreme Court voting example described in Section VI-A. OT 2001 (left column) depicts a typical and relatively non-controversial SCOTUS term, with the raw agreement data (top row) and implied agreement network (bottom row) indicating a high degree of concurrence among the justices. The principal network identified by Network PCA (second column) is a nearly “flat” fully connected network, signifying the high fraction of low-profile but nearly unanimous cases that dominate SCOTUS’s docket. After extracting this factor, the major mode of variation (third column) away from baseline unanimity is a conservative (seats CJ, AJ2, AJ3, AJ4, and AJ6)-liberal (seats AJ1, AJ5, AJ7, AJ8) split among the justices, typical of high-profile “5-4” decisions. Finally, the combination of CUSUM analysis with the CCPD model (right column) identifies the retirement of the moderate Justice O’Connor (seat AJ2) as the most important shift in the OT 1995-OT 2020 time period; the \hat{u} factor from this analysis identifies OT 2005 as the most likely site of the change. Justice O’Connor retired in the middle of OT 2005, suggesting that her successor, Justice Alito, quickly established himself as a significantly more conservative justice than his predecessor. Judicial agreement data for this analysis was extracted from the annual “stat packs” prepared by the legal news and commentary site SCOTUSBlog (scotusblog.com).

We begin by finding the principal (mean) network from this data by applying Algorithm 1 to \mathcal{X} directly. This yields a rank-1 principal component with $\hat{V} \approx \mathbf{1} * 1/3$ or, equivalently, $\hat{V} \circ \hat{V} \approx \mathbf{J}_{9 \times 9} * 1/9$, where \mathbf{J} is the all-ones matrix. This suggests that the baseline behavior of SCOTUS is a broad-based consensus, typified by unanimous or nearly unanimous decisions. While this is somewhat at odds with the popular perception of SCOTUS and news coverage highlighting controversial decisions, it is consistent with the fact that the majority of SCOTUS cases are focused on rather narrow questions of legal and procedural arcana on which the justices can find broad agreement. We also note that the justices have discretion of the majority of their docket and may choose to favor cases where unanimity is likely.

We next apply Network PCA to the residuals from the previous analysis in order to identify the typical patterns of agreement after removing the unanimity factor. In this case, we find a principal network with two clear components of 5 and 4 vertices: a closer examination of this split reveals the prototypical conservative (5) - liberal (4) split, where justices tend to vote in agreement with other justices nominated by a president from the same political party. This factor thus clearly identifies the partisan divide highlighted in media coverage and popular perceptions of SCOTUS. We note, however, that while

the signal of the first factor $\hat{d} \approx 35$ is much stronger than the signal of the second factor $\hat{d} \approx 4.8$ suggesting that public perception is driven by a small number of high-profile and divisive cases.

Finally, we apply a CUSUM type analysis to identify major changes in the voting patterns of SCOTUS justices. The results of this analysis suggest that the most important change—largest element of \hat{u} —occurred in OT 2005 and was driven by the replacement of Justice Sandra Day O’Connor, a moderate conservative who would occasionally vote with her more liberal colleague Justices Souter (seat later held by Justice Sotomayor), by Justice Samuel Alito, a firm conservative who almost always votes in agreement with fellow conservative Justice Thomas. The importance of this shift is commonly noted by legal commentators. We note that, while the replacement of Justice Ruth Bader Ginsberg by Justice Amy Coney Barrett is likely to be even more important in the overall history of the court, Justice Barrett only served for one SCOTUS term in our sample and hence can not be identified by change point analyses. Further, we also note that CUSUM analysis suggests essentially no change in voting behavior when Justice Neil Gorsuch replaced Justice Antonin Scalia, consistent with their similar judicial philosophies and Justice Gorsuch’s adherence to judicial philosophies originally expounded by Justice Scalia.

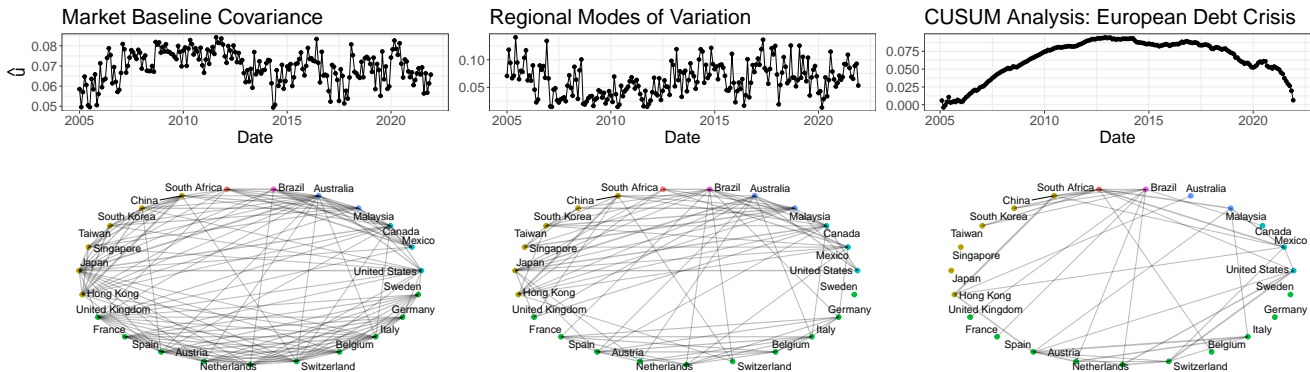


Fig. 5: Application of the CCPD model to the stock market covariance example described in Section VI-B. Baseline market behavior (right column) reflects world-wide economic trends applying to all indices roughly equally; the most significant differences in behavior (center column) capture economic changes in different regions of the world, while the most significant change over time (right column) highlights the divergence of Eurozone stock indices during the European Debt Crisis (major period roughly 2009-2015, though ongoing until 2020). Top row is the estimated time-loading vector \hat{u} which is roughly constant for the global economy factor; bottom row visualizes the estimated networks $\hat{V} \circ \hat{V}$ with small edges thresholded for clarity. Rank- r selected via optimal BIC for each model.

B. Correlation Between National Stock Market Indices

Finally, we apply our CCPD and Network PCA proposals to analyze the behavior of 23 international stock markets, for the period from January 2005 to November 2021. For each month, we construct a 23×23 network with edges given by the correlation among (US Dollar denominated) total returns of national stock market indices. Repeating this process over our time period gives a semi-symmetric tensor of dimension $23 \times 23 \times 204$, each slice of which is positive definite by construction. We then apply the CCPD model in the manner outlined in Section V to identify baseline patterns of market behavior, significant deviations from baseline, and to examine evidence for changes over our 16 year period of interest. Our results are presented in Figure 5.

Not surprisingly, the baseline behavior identified by applying the CCPD to the raw data tensor identifies a baseline network with nearly constant edge strength. This baseline captures the well-known effect of overall market volatility not being isolated in a single market segment or country: this effect is essentially the same as the market or “beta” terms from the Capital Asset Pricing Model and its variants, though here calculated from the CCPD rather than a cross-sectional regression model as is standard in the econometric literature. Examining the associated time loading vector (\hat{u}), we see that the importance of this factor is essentially unchanged throughout our time period. Applying the CCPD again to the residuals of our baseline analysis, we next identify the major patterns that drive deviations from the market-wide factor. As Figure 5 shows, this analysis identifies major geographic regions, implying that, after global effects, the most important market patterns correspond to well-known regional effects (Europe, Asia, and North America). Examining the associated time loading vector, we see that the importance of these regional differences was significantly reduced in the period from 2007 to 2010, roughly capturing the period of the global

financial crisis and the systemic shocks arising in that period.

Finally, we perform a CUSUM analysis on our data to investigate the possibility of market structure changes over our period of interest. While the principal network estimated in this analysis ($\hat{V} \circ \hat{V}$) is less immediately interpretable than those from the previous two analyses, we note that it is primarily concentrated on edges connecting southern European nations, such as Spain and Italy, at the heart of the post-2010 Eurozone debt crisis, with a secondary community centered around China and other rapidly industrializing nations. The CUSUM vector (\hat{u}) shows that the effects of these changes were most pronounced in the period from 2011 to 2016, consistent with the height of Eurozone debt challenges. As we would expect, these effects dissipate rapidly in early 2020 as stock markets began to react to the effects of the COVID-19 pandemic.

VII. DISCUSSION

We have introduced a novel “Coupled CP” tensor decomposition which is tailored to the problem of finding major patterns in semi-symmetric tensors, with a particular focus on tensors arising from multiple observations on a single network. The CCPD extends the classical CP decomposition to allow for low-rank factors in each component while maintaining an easily-interpretable additive structure. To compute this decomposition, we have introduced an efficient alternating minimization algorithm which can be used to estimate a single CCPD factor and a tensor deflation scheme which can be used to extract multiple CCPD factors with restricted orthogonality guarantees. We then establish the statistical consistency of our approach under a semi-symmetric analogue of the classical spiked covariance model and show that it obtains rates on par with the matrix SVD under weak initialization conditions. We describe three different applications of the CCPD in PCA-type procedures, highlighting how it can be used to identify

baseline (first moment) patterns, variance components (second moment), and changepoints. Finally, we demonstrate the efficacy of our decomposition in a simulation study and through examples to SCOTUS voting records and to international stock markets.

While our theoretical and experimental results for the basic CCPD are compelling, we note several directions for future research that may further enhance both our theoretical understanding and the practical usefulness of the decomposition. Matrix-based PCA is known to be inconsistent in high-dimensions without regularization and similar limitations should be expected for the CCPD. As such, a regularized (sparse) CCPD is of significant practical interest, particularly for very large networks where the sample T will almost always be dwarfed by the network size p . We believe our theoretical analysis will extend in a rather straightforward manner to the sparse \mathbf{V} -setting, by using a variant of the truncated power method [25] in lieu of the eigendecomposition in Algorithm 1; alternatively a CCPD-type extension of the unified SF-PCA regularization framework [19] will allow for a wide range of regularization strategies. Computationally, Algorithm 1 exhibits acceptable performance on problems of moderate scale, particularly when combined with the randomization and parallelization schemes discussed in Section II. For problems of larger scale, it is likely to prove necessary to develop more efficient streaming or distributed CCPD algorithms. While much fruitful work considers these types of algorithms in the matrix context, the tensor network context provides additional difficulties in both scale and structure. Finally, it would be interesting to explore analogues of our consistency results under more general generative models than we used, particularly those more tailored to modeling realistic network behaviors.

Acknowledgements

MW's research is supported by an appointment to the Intelligence Community Postdoctoral Research Fellowship Program at the University of Florida Informatics Institute, administered by Oak Ridge Institute for Science and Education through an interagency agreement between the U.S. Department of Energy and the Office of the Director of National Intelligence. GM's research is supported by NSF/DMS grant 1821220. The authors also thank Genevera I. Allen for helpful discussions on the tensor power method.

Proof of Proposition 2

To obtain a deterministic upper-bound on $\|\mathcal{X}\|_{r\text{-op}}$, note

$$\begin{aligned} \|\mathcal{X}\|_{r\text{-op}} &= \max_{\mathbf{u}, \mathbf{V} \in \mathbb{B}^T \times \mathcal{V}^{p \times r}} |([\mathcal{X}; \mathbf{V}], \mathbf{u})| \\ &\leq \max \left| \left\langle \left(\sum \lambda_{\max:r}(\mathcal{X}_{\cdot i}) \right)_i, \mathbf{u} \right\rangle \right| \\ &\leq r \max |(\lambda_{\max}(\mathcal{X}_{\cdot i})_i, \mathbf{u})| \\ &= r \|(\lambda_{\max}(\mathcal{X}_{\cdot i})_i)\|_{\ell_2} \\ &\leq r \sqrt{T} \|(\lambda_{\max}(\mathcal{X}_{\cdot i})_i)\|_{\ell_\infty} \end{aligned}$$

where the first inequality follows from noting that the i^{th} element of $[\mathcal{X}, \mathbf{V}]$ is maximized by the sum of the top r

eigenvalues of the i^{th} slice of \mathcal{X} , the second inequality bounds the sum by r times the maximum, and the third follows from well-known properties of ℓ_p norms on \mathbb{R}^T . To get the stochastic claim, we combine well-known bounds on the operator norm of sub-Gaussian random matrices [43, Corollary 4.4.8] with a union bound over the slices of \mathcal{E} to get a tail bound on $\|\mathcal{E}\|_{r\text{-op}}$:

$$P \left\{ \|\mathcal{E}\|_{r\text{-op}} \lesssim \sigma r \sqrt{T} \left(\sqrt{p} + \sqrt{\log T} + \delta \right) \right\} > 1 - 4e^{-\delta^2}.$$

Proof of Theorem 2

We here give a brief outline of the proof of Theorem 2; the argument leading to Theorem 1 is virtually identical. The heart of our proof an iterative analysis of Algorithm 1 which controls the error in $\mathbf{V}^{(k)}$ in terms of $\mathbf{V}^{(k-1)}$ and repeats this to convergence. Letting $\mathcal{X} = d\mathbf{V}_* \circ \mathbf{V}_* \circ \mathbf{u}_* + \mathcal{E}$, applying the Davis-Kahan theorem [24], [28] to the \mathbf{V} -update

$$\mathbf{V}^{(k+1)} = \text{eigen}(\mathcal{X} \bar{\times}_3 \mathbf{u}^{(k)}),$$

we find

$$\begin{aligned} \|\sin \Theta(\mathbf{V}^*, \mathbf{V}^{(k+1)})\|_F &\leq 2\sqrt{r} |1 - \cos \angle(\mathbf{u}_*, \mathbf{u}^{(k)})| \\ &\quad + 2\sqrt{r} \|\mathcal{E}\|_{r\text{-op}} d. \end{aligned}$$

Similarly, applying the Davis-Kahan theorem to the \mathbf{u} -update

$$\mathbf{u}^{(k+1)} = \text{Norm}([\mathcal{X}, \mathbf{V}^{(k+1)}])$$

yields

$$\begin{aligned} |\sin \angle(\mathbf{u}_*, \mathbf{u}^{(k+1)})| &\leq 2|1 - \langle \mathbf{V}_*, \mathbf{V}^{(k+1)} \rangle^4| \\ &\quad + 4r \|\mathcal{E}\|_{r\text{-op}} d + 2r^2 \|\mathcal{E}\|_{r\text{-op}} d^2 \end{aligned}$$

Due to the non-linear $\text{Norm}(\cdot)$ function, this is not as simple as the \mathbf{V} -update and requires applying the Davis-Kahan theorem to the matrix pair $\tilde{\mathbf{u}}^{(k+1)} \circ \tilde{\mathbf{u}}^{(k+1)}$ and $d^2 \mathbf{u}_* \circ \mathbf{u}_*$, where $\tilde{\mathbf{u}}^{(k+1)} = [\mathcal{X}, \mathbf{V}^{(k+1)}]$ is the pre-normalized iterate. Because $\mathbf{u}^{(k+1)}$ is an eigenvector of $\tilde{\mathbf{u}}^{(k+1)} \circ \tilde{\mathbf{u}}^{(k+1)}$ by construction, the eigenvector bound provided by Davis-Kahan is exactly what is needed to control $\angle(\mathbf{u}_*, \mathbf{u}^{(k+1)})$.

With these two bounds in hand, we can bound the sine of the \mathbf{V} -angle in terms of the cosine of the \mathbf{u} -angle and *vice versa*. To connect these, it suffices to assume we are in the range of angles such that

$$|\sin \theta| \geq 2|1 - \cos \theta|$$

or $\theta \in [0, \tan^{-1}(0.5)] \approx [0, 53.1^\circ]$. In order to ensure a substantial contraction at each step, we make the slightly stronger assumption that

$$\begin{aligned} 2|1 - \cos \theta_{\mathbf{u}_k}| &\leq c_u |\sin \theta_{\mathbf{u}_k}| \\ 2|1 - \cos \theta_{\mathbf{v}_k}| &\leq c_v |\sin \theta_{\mathbf{v}_k}| \end{aligned}$$

for all k and for some fixed $c_u, c_v < 1$. From here, we iterate our \mathbf{u} - and \mathbf{V} -update bounds to show that the error in the \mathbf{u} -iterates is bounded above by

$$|\sin \theta_{\mathbf{u}_k}| \leq (c_u c_v)^k |\sin \theta_{\mathbf{u}_0}| + \frac{8 \|\mathcal{E}\|_{r\text{-op}}}{d} \sum_{i=0}^{k-1} (c_u c_v)^i$$

Taking the $k \rightarrow \infty$ limit, this gives the error bound $\frac{8\|\mathcal{E}\|_{r\text{-op}}}{d(1-c_u c_v)}$ for the final estimate $\hat{\mathbf{u}} = \lim_{k \rightarrow \infty} \mathbf{u}^{(k)}$. Finally, we use Proposition 2 to translate our bounds from $\|\mathcal{E}\|_{r\text{-op}}$ to bounds in terms of the sub-Gaussian parameter σ .

An important technical element of our proof is to ensure that the iterates remain within the strict (c_u, c_v) -contraction region for all k . While this follows immediately for the noiseless case, the noisy case is more subtle, requiring us to balance the non-expansive error from our initialization with the effect of the noise \mathcal{E} which recurs at each iteration. To ensure this, we need our iterates to be bounded away from the boundary of the contraction region so that the sequence of “contract + add noise” does not increase the total error at any iterate. We term this non-expansive region the “stable interior” of the contraction region. Simple algebra shows that assuming assuming $\theta_{\mathbf{u}_k}$ is in the stable interior, *i.e.*,

$$|1 - \cos \theta_{\mathbf{u}_k}| \leq \tan^{-1}(0.5) - \frac{5\|\mathcal{E}\|_{r\text{-op}}}{d(1 - c_u c_v)},$$

implies that $\theta_{\mathbf{u}_{k+1}}$ is in the stable interior so it suffices to make this stronger assumption on the initialization $\theta_{\mathbf{u}_0}$ only.

REFERENCES

- [1] I. T. Jolliffe, *Principal Component Analysis*, 2nd. 2002. DOI: [10.1007/b98835](https://doi.org/10.1007/b98835).
- [2] B. W. Silverman, “Smoothed functional principal components analysis by choice of norm,” *Annals of Statistics*, vol. 24, no. 1, pp. 1–24, 1996. DOI: [10.1214/aos/1033066196](https://doi.org/10.1214/aos/1033066196).
- [3] L. T. Liu, E. Dobriban, and A. Singer, “ePCA: High-dimensional exponential family PCA,” *Annals of Applied Statistics*, vol. 12, no. 4, pp. 2121–2150, 2018. DOI: [10.1214/18-AOAS1146](https://doi.org/10.1214/18-AOAS1146).
- [4] S. Jung, I. L. Dryden, and J. S. Marron, “Analysis of principal nested spheres,” *Biometrika*, vol. 99, no. 3, pp. 551–568, 2012. DOI: [10.1093/biomet/ass022](https://doi.org/10.1093/biomet/ass022).
- [5] Z. Zhang, G. I. Allen, H. Zhu, and D. Dunson, “Tensor network factorizations: Relationships between brain structural connectomes and traits,” *NeuroImage*, vol. 197, pp. 330–343, 2019. DOI: [10.1016/j.neuroimage.2019.04.027](https://doi.org/10.1016/j.neuroimage.2019.04.027).
- [6] M. Navarro, G. I. Allen, and M. Weylandt, “Network clustering for latent state and changepoint detection,” *ArXiv Pre-Print 2111.01273*, 2021. [Online]. Available: <https://arxiv.org/abs/2111.01273>.
- [7] L. Wang, L. Albera, A. Kachenoura, H. Z. Shu, and L. Senhadji, “CP decomposition of semi-nonnegative semi-symmetric tensors based on QR matrix factorization,” in *SAM 2014: Proceedings of the 8th IEEE Sensor Array and Multichannel Signal Processing Workshop (SAM)*, 2014, pp. 449–452. DOI: [10.1109/SAM.2014.6882439](https://doi.org/10.1109/SAM.2014.6882439).
- [8] T. G. Kolda, “Numerical optimization for symmetric tensor decomposition,” *Mathematical Programming*, vol. 151, pp. 225–248, 2015. DOI: [10.1007/s10107-015-0895-0](https://doi.org/10.1007/s10107-015-0895-0).
- [9] T. G. Kolda and B. W. Bader, “Tensor decompositions and applications,” *SIAM Review*, vol. 51, no. 3, pp. 455–500, 2009. DOI: [10.1137/07070111X](https://doi.org/10.1137/07070111X).
- [10] A. Zare, A. Ozdemir, M. A. Iwen, and S. Aviyente, “Extension of PCA to higher order data structures: An introduction to tensors, tensor decompositions, and tensor PCA,” *Proceedings of the IEEE*, vol. 106, no. 8, pp. 1341–1358, 2018. DOI: [10.1109/JPROC.2018.2848209](https://doi.org/10.1109/JPROC.2018.2848209).
- [11] G. I. Allen, “Multi-way functional principal components analysis,” in *CAMSAP 2013: Proceedings of the 5th IEEE International Workshop on Computational Advances in Multi-Sensor Adaptive Processing*, 2013, pp. 220–223. DOI: [10.1109/CAMSAP.2013.6714047](https://doi.org/10.1109/CAMSAP.2013.6714047).
- [12] —, “Sparse higher-order principal components analysis,” in *AISTATS 2012: Proceedings of the 15th International Conference on Artificial Intelligence and Statistics*, vol. 22, 2012, pp. 27–36. [Online]. Available: <http://proceedings.mlr.press/v22/allen12.html>.
- [13] A. Athreya, D. E. Fishkind, M. Tang, C. E. Priebe, Y. Park, J. T. Vogelstein, K. Levin, V. Lyzinski, Y. Qin, and D. L. Sussman, “Statistical inference on random dot product graphs: A survey,” *Journal of Machine Learning Research*, vol. 18, no. 226, pp. 1–92, 2018. [Online]. Available: <http://jmlr.org/papers/v18/17-448.html>.
- [14] D. L. Sussman, M. Tang, and C. E. Priebe, “Consistent latent position estimation and vertex classification for random dot product graphs,” *IEEE Transactions on Pattern Analysis and Machine Intelligence*, vol. 36, no. 1, pp. 48–57, 2014. DOI: [10.1109/TPAMI.2013.135](https://doi.org/10.1109/TPAMI.2013.135).
- [15] V. Lyzinski, M. Tang, A. Athreya, Y. Park, and C. E. Priebe, “Community detection and classification in hierarchical stochastic blockmodels,” *IEEE Transactions on Network Science and Engineering*, vol. 4, no. 1, pp. 13–26, 2016. DOI: [10.1109/TNSE.2016.2634322](https://doi.org/10.1109/TNSE.2016.2634322).
- [16] P. A. Regalia and E. Kofidis, “The higher-order power method revisited: Convergence proofs and effective initialization,” in *ICASSP 2000: Proceedings of the 2000 IEEE International Conference on Acoustics, Speech, and Signal Processing*, vol. 5, pp. 2709–2712. DOI: [10.1109/ICASSP.2000.861047](https://doi.org/10.1109/ICASSP.2000.861047).
- [17] E. Kofidis and P. A. Regalia, “On the best rank-1 approximation of higher-order supersymmetric tensors,” *SIAM Journal on Matrix Analysis and Applications*, vol. 23, no. 3, pp. 863–884, 2002. DOI: [10.1137/S0895479801387413](https://doi.org/10.1137/S0895479801387413).
- [18] L. Mackey, “Deflation methods for sparse PCA,” in *NIPS 2008: Advances in Neural Information Processing Systems 21*, 2008, pp. 1017–1024. [Online]. Available: <https://papers.nips.cc/paper/3575-deflation-methods-for-sparse-pca>.
- [19] M. Weylandt, “Multi-rank sparse and functional PCA: Manifold optimization and iterative deflation techniques,” in *CAMSAP 2019: Proceedings of the 8th IEEE Workshop on Computational Advances in Multi-Sensor Adaptive Processing*, 2019, pp. 500–504. DOI: [10.1109/CAMSAP45676.2019.9022486](https://doi.org/10.1109/CAMSAP45676.2019.9022486).

- [20] N. Halko, P.-G. Martinsson, and J. A. Tropp, “Finding structure with randomness: Probabilistic algorithms for constructing approximate matrix decompositions,” *SIAM Review*, vol. 53, no. 2, pp. 217–288, 2011. DOI: [10.1137/090771806](https://doi.org/10.1137/090771806).
- [21] E. T. Phipps and T. G. Kolda, “Software for sparse tensor decomposition on emerging computing architectures,” *SIAM Journal on Scientific Computing*, vol. 41, no. 3, pp. C269–290, 2019. DOI: [10.1137/18M1210691](https://doi.org/10.1137/18M1210691).
- [22] S. Zhang, V. Karihaloo, and P. Wu, “Basic linear algebra operations on TensorCore GPU,” in *ScalA 2020: Proceedings of the 11th IEEE/ACM 11 Workshop on Latest Advances in Scalable Algorithms for Large-Scale Systems*, 2020, pp. 44–52. DOI: [10.1109/ScalA51936.2020.00011](https://doi.org/10.1109/ScalA51936.2020.00011).
- [23] J. Fan, H. Liu, Q. Sun, and T. Zhang, “I-LAMM for sparse learning: Simultaneous control of algorithmic complexity and statistical error,” *Annals of Statistics*, vol. 46, no. 2, pp. 814–841, 2018. DOI: [10.1214/17-AOS1568](https://doi.org/10.1214/17-AOS1568).
- [24] Y. Yu, T. Wang, and R. J. Samworth, “A useful variant of the Davis–Kahan theorem for statisticians,” *Biometrika*, vol. 102, no. 2, pp. 315–323, 2015. DOI: [10.1093/biomet/asv008](https://doi.org/10.1093/biomet/asv008).
- [25] X.-T. Yuan and T. Zhang, “Truncated power method for sparse eigenvalue problems,” *Journal of Machine Learning Research*, vol. 14, no. Apr, pp. 899–925, 2013. [Online]. Available: <http://www.jmlr.org/papers/v14/yuan13a.html>.
- [26] K. Lounici, “Sup-norm convergence rate and sign concentration property of Lasso and Dantzig estimators,” *Electronic Journal of Statistics*, vol. 2, pp. 90–102, 2008, ISSN: 1935-7524. DOI: [10.1214/08-EJS177](https://doi.org/10.1214/08-EJS177).
- [27] M. Hardt and E. Price, “The noisy power method: A meta algorithm with applications,” in *NIPS 2014: Advances in Neural Information Processing Systems 27*, 2014. [Online]. Available: <https://proceedings.neurips.cc/paper/2014/hash/729c68884bd359ade15d5f163166738a-Abstract.html>.
- [28] C. Davis and W. M. Kahan, “The rotation of eigenvectors by a perturbation III,” *SIAM Journal on Numerical Analysis*, vol. 7, no. 1, pp. 1–46, 1970. DOI: [10.1137/0707001](https://doi.org/10.1137/0707001).
- [29] W. W. Sun, J. Lu, H. Liu, and G. Cheng, “Provable sparse tensor decomposition,” *Journal of the Royal Statistical Society, Series B: Statistical Methodology*, vol. 79, no. 3, pp. 899–916, 2017. DOI: [10.1111/rssb.12190](https://doi.org/10.1111/rssb.12190).
- [30] K. Chaudhuri, F. Chung, and A. Tsiatas, “Spectral clustering of graphs with general degrees in the extended planted partition model,” in *COLT 2012: Proceedings of the 25th Annual Conference on Learning Theory*, vol. 23, 2012, pp. 35.1–35.23. [Online]. Available: <https://proceedings.mlr.press/v23/chaudhuri12.html>.
- [31] R. B. Cattell, “The scree test for the number of factors,” *Multivariate Behavioral Research*, vol. 1, no. 2, pp. 245–276, 1966. DOI: [10.1207/s15327906mbr0102_10](https://doi.org/10.1207/s15327906mbr0102_10).
- [32] A. B. Owen and P. O. Perry, “Bi-cross-validation of the SVD and the nonnegative matrix factorization,” *Annals of Applied Statistics*, vol. 3, no. 2, pp. 564–594, 2009. DOI: [10.1214/08-AOAS227](https://doi.org/10.1214/08-AOAS227).
- [33] J. Josse and F. Husson, “Selecting the number of components in principal component analysis using cross-validation approximations,” *Computational Statistics & Data Analysis*, vol. 56, no. 6, pp. 1869–1879, 2012. DOI: [10.1016/j.csda.2011.11.012](https://doi.org/10.1016/j.csda.2011.11.012).
- [34] Y. Choi, J. Taylor, and R. Tibshirani, “Selecting the number of principal components: Estimation of the true rank of a noisy matrix,” *Annals of Statistics*, vol. 45, no. 6, pp. 2590–2617, 2017. DOI: [10.1214/16-AOS1536](https://doi.org/10.1214/16-AOS1536).
- [35] Z. Bai, K. P. Choi, and Y. Fujikoshi, “Consistency of AIC and BIC in estimating the number of significant components in high-dimensional principal component analysis,” *Annals of Statistics*, vol. 46, no. 3, pp. 1050–1076, 2018. DOI: [10.1214/17-AOS1577](https://doi.org/10.1214/17-AOS1577).
- [36] F. Sedighin, A. Cichocki, and A.-H. Phan, “Adaptive rank selection for tensor ring decomposition,” *IEEE Journal of Selected Topics in Signal Processing*, vol. 15, no. 3, pp. 454–463, 2021. DOI: [10.1109/JSTSP.2021.3051503](https://doi.org/10.1109/JSTSP.2021.3051503).
- [37] M. Journée, Y. Nesterov, P. Richtárik, and R. Sepulchre, “Generalized power method for sparse principal component analysis,” *Journal of Machine Learning Research*, vol. 11, pp. 517–553, 2010. [Online]. Available: <http://www.jmlr.org/papers/v11/journee10a.html>.
- [38] Y. Kawakami and M. Sugiyama, “Investigating overparameterization for non-negative matrix factorization in collaborative filtering,” in *RecSys 21: Proceedings of the Fifteenth ACM Conference on Recommender Systems*, 2021, pp. 685–690. DOI: [10.1145/3460231.3478854](https://doi.org/10.1145/3460231.3478854).
- [39] H. Xu, C. Caramanis, and S. Sanghavi, “Robust PCA via outlier pursuit,” *IEEE Transactions on Information Theory*, vol. 58, no. 5, pp. 3047–3064, 2012. DOI: [10.1109/TIT.2011.2173156](https://doi.org/10.1109/TIT.2011.2173156).
- [40] T. Wang and R. J. Samworth, “High dimensional change point estimation via sparse projection,” *Journal of the Royal Statistical Society, Series B: Statistical Methodology*, vol. 80, no. 1, pp. 57–83, 2018. DOI: [10.1111/rssb.12243](https://doi.org/10.1111/rssb.12243).
- [41] D. Wang, Y. Yu, and A. Rinaldo, “Univariate mean change point detection: Penalization, CUSUM and optimality,” *Electronic Journal of Statistics*, vol. 14, pp. 1917–1961, 2020, ISSN: 1935-7524. DOI: [10.1214/20-EJS1710](https://doi.org/10.1214/20-EJS1710).
- [42] —, “Optimal change point detection and localization in sparse dynamic networks,” *Annals of Statistics*, vol. 49, no. 1, pp. 203–232, 2021. DOI: [10.1214/20-AOS1953](https://doi.org/10.1214/20-AOS1953).
- [43] R. Vershynin, *High-Dimensional Probability: An Introduction with Applications in Data Science*, 1st. 2018.

SUPPLEMENTAL MATERIALS

PROOFS

In this section, we present the complete proofs of Theorems 1 and 2, giving more detail than in the main text above. Before proceeding, we state for completeness the variant of the Davis-Kahan (1970) theorem due to Yu, Wang, and Samworth [2], specialized for our case:

Proposition 3. *Suppose $\Sigma^* \in \mathbb{R}_{\geq 0}^{p \times p}$ has rank $r < p$ and has all non-zero eigenvalues at least $\lambda > 0$. Suppose further that $\hat{\Sigma} = \Sigma^* + \mathbf{E}$ is an estimate of Σ^* . Then*

$$\|\sin \Theta(\mathbf{V}^*, \hat{\mathbf{V}})\|_F \leq \frac{2r^{1/2} \|\mathbf{E}\|_{op}}{\lambda}$$

where $\mathbf{V}^*, \hat{\mathbf{V}}$ are matrices composed of the r leading eigenvectors of $\mathbf{V}^*, \hat{\mathbf{V}}$ respectively and $\Theta(\mathbf{V}^*, \hat{\mathbf{V}})$ denotes the $r \times r$ diagonal matrix whose entries are the principal angles between the spaces spanned \mathbf{V}^* and $\hat{\mathbf{V}}$ and where $\sin(\cdot)$ is applied elementwise. Furthermore, there exists an orthogonal matrix $\mathbf{O} \in \mathcal{V}^{r \times r}$ such that

$$\|\mathbf{V}^* - \hat{\mathbf{V}}\mathbf{O}\|_F \leq \frac{2^{3/2}r^{1/2} \|\mathbf{E}\|_{op}}{\lambda}.$$

Proof. This proof follows immediately from Theorem 1 of Yu, Wang, and Samworth [2], with r, s, d in their notation being equal to $1, r, r$ in our notation. The denominator of their bound is

$$\min(\lambda_0(\Sigma^*) - \lambda_1(\Sigma^*), \lambda_r(\Sigma^*) - \lambda_{r+1}(\Sigma^*)) \geq \min(\infty - \lambda, \lambda - 0) = \lambda,$$

which gives the denominator in our statement above. Finally, we use only the operator norm bound on \mathbf{E} as it is easier to analyze under our noise model, but the Frobenius norm could be used as well. \square

With this result in hand, we are able to prove Theorem 1. To simplify the proof, we first establish the following non-stochastic lemma:

Lemma 1. *Suppose $\mathcal{X} = d\mathbf{V}_* \circ \mathbf{V}_* \circ \mathbf{u}_* + \mathcal{E}$ for a unit-norm T -vector \mathbf{u}_* , a $p \times r$ orthogonal matrix \mathbf{V}_* satisfying $\mathbf{V}_*^T \mathbf{V}_* = \mathbf{I}_{r \times r}$, $r \in \mathbb{R}_{\geq 0}$, and $\mathcal{E} \in \mathbb{R}^{p \times p \times T}$ a semi-symmetric tensor. Then the result of Algorithm 1 applied to \mathcal{X} satisfies the following:*

$$\begin{aligned} \min_{\epsilon = \pm 1} \|\epsilon \mathbf{u}^* - \mathbf{u}^*\|_2 &\leq \frac{8\sqrt{2} \|\mathcal{E}\|_{r-op}}{d(1-c)} \\ \|\mathbf{V}^* \mathbf{O} - \hat{\mathbf{V}}\|_F &\leq \frac{8\sqrt{2}r \|\mathcal{E}\|_{r-op}}{d(1-c)} \end{aligned}$$

so long as $\|\mathcal{E}\|_{r-op} < d$ and

$$|1 - \langle \mathbf{u}_0, \mathbf{u}_* \rangle| \leq \tan^{-1}(0.5) - \frac{5 \|\mathcal{E}\|_{r-op}}{d(1-c)}$$

for some arbitrary $c < 1$.

The structure of our proof is straight-forward: we use the Davis-Kahan theorem to analyze a single iteration of the \mathbf{V} and \mathbf{u} -update steps of Algorithm 1, showing that the error at each step can be bounded by a sum of a term depending on the error from the previous iteration and a term depending on $\|\mathcal{E}\|_{r-op}/d$. Under some conditions which can be interpreted as being in a ‘‘basin of attraction,’’ we show that the iterates contract to a small ball around \mathbf{V}_* and \mathbf{u}_* . Finally, we show that the initialization condition on \mathbf{u}_0 and some assumptions on the relative magnitude of $\|\mathcal{E}\|_{r-op}$ and d suffice to ensure that all iterates remain in the basin of attraction. Combining these steps, we obtain a proof of Lemma 1

Proof. For simplicity, and with minimal loss of generality, we specialize our proof to the rank-1 case. Comments on the general rank- r case appear at the end of each section of the proof.

Our proof proceeds in four parts:

- I. Analysis of the \mathbf{V} -Update
- II. Analysis of the \mathbf{u} -Update
- III. Iterative Error Analysis
- IV. Condition Checking

I. Analysis of \mathbf{v} -Update. Recall that, in the rank-1 case, the \mathbf{v} -update is given by

$$\mathbf{v}^{(k+1)} = \text{eigen}(\mathcal{X} \bar{\times}_3 \mathbf{u}^{(k)})$$

where $\text{eigen}(\cdot)$ denotes the leading eigenvector. Under our model, this can be simplified as

$$\mathcal{X} \bar{\times}_3 \mathbf{u}^{(k)} = (d\langle \mathbf{u}_*, \mathbf{u}^{(k)} \rangle) \mathbf{v}_* \circ \mathbf{v}_* + \mathcal{E} \bar{\times}_3 \mathbf{u}^{(k)}$$

We apply Proposition 3 with $\Sigma^* = d\mathbf{v}_* \circ \mathbf{v}_*$ and $\hat{\Sigma} = \mathcal{X} \bar{\times}_3 \mathbf{u}^{(k)}$. This implies $\mathbf{E} = d(\langle \mathbf{u}^{(k)}, \mathbf{u}_* \rangle - 1)\mathbf{v}_* \circ \mathbf{v}_* + \mathcal{E} \bar{\times}_3 \mathbf{u}^{(k)}$ and hence

$$\begin{aligned} \|\mathbf{E}\|_{\text{op}} &= \left\| d(\langle \mathbf{u}^{(k)}, \mathbf{u}_* \rangle - 1)\mathbf{v}_* \circ \mathbf{v}_* + \mathcal{E} \bar{\times}_3 \mathbf{u}^{(k)} \right\|_{\text{op}} \\ &\leq |d| \left| \langle \mathbf{u}^{(k)}, \mathbf{u}_* \rangle - 1 \right| \|\mathbf{v}_* \circ \mathbf{v}_*\|_{\text{op}} + \|\mathcal{E} \bar{\times}_3 \mathbf{u}^{(k)}\|_{\text{op}} \\ &\leq d \left| \langle \mathbf{u}^{(k)}, \mathbf{u}_* \rangle - 1 \right| + \|\mathcal{E}\|_{\text{op}} \end{aligned}$$

Hence Proposition 3 implies

$$|\sin \angle(\mathbf{v}^*, \mathbf{v}^{(k+1)})| \leq 2 \left| \langle \mathbf{u}^{(k)}, \mathbf{u}_* \rangle - 1 \right| + \frac{2\|\mathcal{E}\|_{\text{op}}}{d}$$

The extension to the rank- r case is straight-forward:

$$\left\| \sin \Theta(\mathbf{v}^*, \mathbf{v}^{(k+1)}) \right\|_F \leq 2\sqrt{r} \left| \langle \mathbf{u}^{(k)}, \mathbf{u}_* \rangle - 1 \right| + \frac{2\sqrt{r}\|\mathcal{E}\|_{r\text{-op}}}{d}$$

The only noteworthy change is an additional \sqrt{r} -term arising in the final Davis-Kahan bound.

II. Analysis of \mathbf{u} -Update. Recall that the \mathbf{u} -update is given by

$$\mathbf{u}^{(k+1)} = \text{Norm}([\mathcal{X}; \mathbf{V}^{(k+1)}])$$

In the rank-1 case, this can be rewritten and simplified as

$$\begin{aligned} \mathbf{u}^{(k+1)} &= \text{Norm}([\mathcal{X}; \mathbf{V}^{(k+1)}]) \\ &= \text{Norm}([d\mathbf{v}_* \circ \mathbf{v}_* \circ \mathbf{u}_* + \mathcal{E}; \mathbf{v}^{(k+1)}]) \\ &= \text{Norm}(d[\mathbf{v}_* \circ \mathbf{v}_* \circ \mathbf{u}_*; \mathbf{v}^{(k+1)}] + [\mathcal{E}; \mathbf{v}^{(k+1)}]) \\ &= \text{Norm}(d\mathbf{v}_* \circ \mathbf{v}_* \circ \mathbf{u}_* \bar{\times}_1 \mathbf{v}^{(k+1)} \bar{\times}_2 \mathbf{v}^{(k+1)} + \mathcal{E} \bar{\times}_1 \mathbf{v}^{(k+1)} \bar{\times}_2 \mathbf{v}^{(k+1)}) \\ &= \text{Norm} \left(\underbrace{d\mathbf{u}_* |\langle \mathbf{v}_*, \mathbf{v}^{(k+1)} \rangle|^2 + \mathcal{E} \bar{\times}_1 \mathbf{v}^{(k+1)} \bar{\times}_2 \mathbf{v}^{(k+1)}}_{=\tilde{\mathbf{u}}^{(k+1)}} \right) \end{aligned}$$

The non-linear normalization step makes this quantity to analyze directly, but we can circumvent it by a ‘‘reverse’’ use of the Davis-Kahan theorem. By construction, $\mathbf{u}^{(k+1)}$ is the leading eigenvector of $\tilde{\mathbf{u}}^{(k+1)} \circ \tilde{\mathbf{u}}^{(k+1)}$ and \mathbf{u}_* is the leading eigenvector of $d^2\mathbf{u}_* \circ \mathbf{u}_*$. Note that

$$\tilde{\mathbf{u}}^{(k+1)} \circ \tilde{\mathbf{u}}^{(k+1)} = (d')^2 \mathbf{u}_* \circ \mathbf{u}_* + d'\mathbf{u}_* \circ \mathbf{e} + d'\mathbf{e} \circ \mathbf{u}_* + \mathbf{e} \circ \mathbf{e}$$

where $d' = d|\langle \mathbf{v}_*, \mathbf{v}^{(k+1)} \rangle|^2$ and $\mathbf{e} = \mathcal{E} \bar{\times}_1 \mathbf{v}^{(k+1)} \bar{\times}_2 \mathbf{v}^{(k+1)}$. Plugging these into Proposition 3, we have

$$\begin{aligned} \|\mathbf{E}\|_{\text{op}} &= \left\| d^2\mathbf{u}_* \circ \mathbf{u}_* - \tilde{\mathbf{u}}^{(k+1)} \circ \tilde{\mathbf{u}}^{(k+1)} \right\| \\ &= \left\| d^2(1 - \langle \mathbf{v}_*, \mathbf{v}^{(k+1)} \rangle^4)\mathbf{u}_* \circ \mathbf{u}_* + d'\mathbf{u}_* \circ \mathbf{e} + d'\mathbf{e} \circ \mathbf{u}_* + \mathbf{e} \circ \mathbf{e} \right\|_{\text{op}} \\ &\leq d^2|1 - \langle \mathbf{v}_*, \mathbf{v}^{(k+1)} \rangle^4| \|\mathbf{u}_* \circ \mathbf{u}_*\|_{\text{op}} + 2d' \|\mathbf{u}_* \circ \mathbf{e}\|_{\text{op}} + \|\mathbf{e} \circ \mathbf{e}\|_{\text{op}} \\ &\leq d^2|1 - \langle \mathbf{v}_*, \mathbf{v}^{(k+1)} \rangle^4| \|\mathbf{u}_*\|^2 + 2d' \|\mathbf{u}_*\| \|\mathbf{e}\| + \|\mathbf{e}\|^2 \end{aligned}$$

which implies

$$\begin{aligned} |\sin \angle(\mathbf{u}_*, \mathbf{u}^{(k+1)})| &\leq \frac{2\|\mathbf{E}\|_{\text{op}}}{d^2} \\ &\leq \frac{2[d^2|1 - \langle \mathbf{v}_*, \mathbf{v}^{(k+1)} \rangle^4| \|\mathbf{u}_*\|^2 + 2d' \|\mathbf{u}_*\| \|\mathbf{e}\| + \|\mathbf{e}\|^2]}{d^2} \\ &= 2|1 - \langle \mathbf{v}_*, \mathbf{v}^{(k+1)} \rangle^4| + \frac{4d' \|\mathbf{e}\|}{d^2} + \frac{2\|\mathbf{e}\|^2}{d^2} \\ &\leq 2|1 - \langle \mathbf{v}_*, \mathbf{v}^{(k+1)} \rangle^4| + \frac{4\|\mathcal{E}\|_{\text{op}}}{d} + \frac{2\|\mathcal{E}\|_{\text{op}}^2}{d^2} \end{aligned}$$

where the final inequality follows from the fact that $d' = d(1 - \langle \mathbf{v}_*, \mathbf{v}^{(k+1)} \rangle^2) < d$ and $\|\mathbf{e}\| = \|\mathcal{E} \bar{\times}_1 \mathbf{v}^{(k+1)} \bar{\times}_2 \mathbf{v}^{(k+1)}\| \leq \|\mathcal{E}\|_{\text{op}}$.

This is step of the proof requiring the most cumbersome algebra, and hence the hardest to extend to the rank- r case. The major difficulty is in substituting the $[\mathcal{X}, \mathbf{V}^{(k+1)}]$ for the simpler $\mathcal{X} \bar{\times}_1 \mathbf{v}^{(k+1)} \bar{\times}_2 \mathbf{v}^{(k+1)}$ construction, but both are linear in the \mathcal{X} argument and the same argument essentially holds, with the normalized Frobenius inner product on matrices $\langle \mathbf{A}, \mathbf{B} \rangle =$

$\text{Tr}(\mathbf{A}^T \mathbf{B})/r$ taking the place of the Euclidean inner product. This gives the error bound:

$$|\sin \angle(\mathbf{u}_*, \mathbf{u}^{(k+1)})| \leq 2(1 - \langle \mathbf{V}_*, \mathbf{V}^{(k+1)} \rangle^4) + \frac{4r \|\mathcal{E}\|_{\text{op}}}{d} + \frac{2r^2 \|\mathcal{E}\|_{r\text{-op}}^2}{d^2}$$

where the $\|\mathcal{E}\|_{r\text{-op}}$ terms are scaled by r to account for the fact that we are now using r vectors instead of just one. Note that the Davis-Kahan bound does not pick up an extra \sqrt{r} since the \mathbf{u} factor remains univariate even in the rank- r decomposition.

III. Iterative Error Analysis. The previous two parts gave us the following accuracy bounds:

$$\begin{aligned} |\sin \angle(\mathbf{v}^*, \mathbf{v}^{(k+1)})| &\leq 2 \left| \langle \mathbf{u}^{(k)}, \mathbf{u}_* \rangle - 1 \right| + \frac{2 \|\mathcal{E}\|_{\text{op}}}{d} \\ |\sin \angle(\mathbf{u}_*, \mathbf{u}^{(k+1)})| &\leq 2(1 - \langle \mathbf{v}_*, \mathbf{v}^{(k+1)} \rangle^4) + \frac{4 \|\mathcal{E}\|_{\text{op}}}{d} + \frac{2 \|\mathcal{E}\|_{\text{op}}^2}{d^2} \end{aligned}$$

or equivalently:

$$|\sin \theta_{\mathbf{v}_{k+1}}| \leq 2|1 - \cos \theta_{\mathbf{u}_k}| + \frac{2 \|\mathcal{E}\|_{\text{op}}}{d} \quad (\text{A1})$$

$$|\sin \theta_{\mathbf{u}_{k+1}}| \leq 2|1 - \cos^4 \theta_{\mathbf{v}_{k+1}}| + \frac{4 \|\mathcal{E}\|_{\text{op}}}{d} + \frac{2 \|\mathcal{E}\|_{\text{op}}^2}{d^2} \quad (\text{A2})$$

where $\theta_{\mathbf{v}_k} = \angle(\mathbf{v}^{(k)}, \mathbf{v}_*) = \cos^{-1} \langle \mathbf{v}^{(k)}, \mathbf{v}_* \rangle$ and similarly for $\theta_{\mathbf{u}_k}$. This suggests that, under some conditions, the sequence of iterates can contract to the true solution ($\theta = 0$): specifically, in the noiseless ($\mathcal{E} = 0$) case, we recall that

$$2|1 - \cos \theta| \leq |\sin \theta| \quad \text{for all } |\theta| \in [0, 2 \tan^{-1}(0.5) \approx [0^\circ, 53.1^\circ]]$$

In low-dimensions, this condition can typically be obtained by random initialization; in moderate- to high-dimensional settings, a more nuanced initialization is required. Under this “shrinkage” condition, the proof follows by repeated substitution of Equations (A1-A2) into each other.

The extension to the noisy case is more difficult. It does not suffice for the passage between $\sin(\cdot)$ and $\cos(\cdot)$ to be non-contractive, because the effect of the noise term $\|\mathcal{E}\|_{\text{op}}$ can accumulate over repeated iterations. To handle the noisy case, we require a strict contraction at each step. Specifically, we assume that:

$$\begin{aligned} 2|1 - \cos \theta_{\mathbf{u}_k}| &\leq c_u |\sin \theta_{\mathbf{u}_k}| \quad \text{for all } k, \text{ for some } c_u < 1 \\ 2|1 - \cos^4 \theta_{\mathbf{v}_k}| &\leq c_v |\sin \theta_{\mathbf{v}_k}| \quad \text{for all } k, \text{ for some } c_v < 1. \end{aligned} \quad (\text{A3})$$

Then we have the following bounds for the \mathbf{v} iterates:

$$\begin{aligned} |\sin \theta_{\mathbf{v}_{k+1}}| &\leq 2|1 - \cos \theta_{\mathbf{u}_k}| + \frac{2 \|\mathcal{E}\|_{\text{op}}}{d} \\ &\leq c_u |\sin \theta_{\mathbf{u}_k}| + \frac{2 \|\mathcal{E}\|_{\text{op}}}{d} \\ &\leq c_u \left(2|1 - \cos^4 \theta_{\mathbf{v}_k}| + \frac{4 \|\mathcal{E}\|_{\text{op}}}{d} + \frac{2 \|\mathcal{E}\|_{\text{op}}^2}{d^2} \right) + \frac{2 \|\mathcal{E}\|_{\text{op}}}{d} \\ &\leq c_u c_v |\sin \theta_{\mathbf{v}_k}| + \frac{4c_u \|\mathcal{E}\|_{\text{op}}}{d} + \frac{2c_u \|\mathcal{E}\|_{\text{op}}^2}{d^2} + \frac{2 \|\mathcal{E}\|_{\text{op}}}{d} \end{aligned} \quad (\text{A4})$$

Iterating this, we find that:

$$|\sin \theta_{\mathbf{v}_k}| \leq (c_u c_v)^k |\sin \theta_{\mathbf{v}_1}| + \left(\frac{4c_u \|\mathcal{E}\|_{\text{op}}}{d} + \frac{2c_u \|\mathcal{E}\|_{\text{op}}^2}{d^2} + \frac{2 \|\mathcal{E}\|_{\text{op}}}{d} \right) \sum_{i=0}^{k-1} (c_u c_v)^i$$

We highlight here that the convergence of the non-stochastic part of the error is geometric in $c_u c_v$. Letting $k \rightarrow \infty$, the first

term vanishes and the second term can be simplified as

$$\begin{aligned}
|\sin \theta_{\mathbf{v}_k}| &\leq \frac{1}{1 - c_u c_v} \left(\frac{4c_u \|\mathcal{E}\|_{\text{op}}}{d} + \frac{2c_u \|\mathcal{E}\|_{\text{op}}^2}{d^2} + \frac{2 \|\mathcal{E}\|_{\text{op}}}{d} \right) \\
&\leq \frac{6 \frac{\|\mathcal{E}\|_{\text{op}}}{d} + 2 \frac{\|\mathcal{E}\|_{\text{op}}^2}{d^2}}{1 - c_u c_v} \\
&\leq \frac{6 \frac{\|\mathcal{E}\|_{\text{op}}}{d} + 2 \frac{\|\mathcal{E}\|_{\text{op}}}{d}}{1 - c_u c_v} \\
&= \frac{8 \|\mathcal{E}\|_{\text{op}}}{d(1 - c_u c_v)}
\end{aligned}$$

when $\frac{\|\mathcal{E}\|_{\text{op}}}{d} < 1$. Interestingly, the explicit term measuring the quality of the initialization ($\sin \theta_{\mathbf{v}_0}$) vanishes, but the quality of the initialization persists in the c_u and c_v terms.

Bounds for the \mathbf{u} iterates can be attained similarly:

$$\begin{aligned}
|\sin \theta_{\mathbf{u}_k}| &\leq 2|1 - \cos^4 \theta_{\mathbf{v}_k}| + \frac{4 \|\mathcal{E}\|_{\text{op}}}{d} + \frac{2 \|\mathcal{E}\|_{\text{op}}^2}{d^2} \\
&\leq c_v |\sin \theta_{\mathbf{v}_k}| + \frac{4 \|\mathcal{E}\|_{\text{op}}}{d} + \frac{2 \|\mathcal{E}\|_{\text{op}}^2}{d^2} \\
&\leq c_v \left(2|1 - \cos \theta_{\mathbf{u}_{k-1}}| + \frac{2 \|\mathcal{E}\|_{\text{op}}}{d} \right) + \frac{4 \|\mathcal{E}\|_{\text{op}}}{d} + \frac{2 \|\mathcal{E}\|_{\text{op}}^2}{d^2} \\
&\leq c_u c_v |\sin \theta_{\mathbf{u}_{k-1}}| + \frac{2c_v \|\mathcal{E}\|_{\text{op}}}{d} + \frac{4 \|\mathcal{E}\|_{\text{op}}}{d} + \frac{2 \|\mathcal{E}\|_{\text{op}}^2}{d^2}
\end{aligned}$$

Iterating, this yields:

$$|\sin \theta_{\mathbf{u}_k}| \leq (c_u c_v)^k |\sin \theta_{\mathbf{u}_0}| + \left(\frac{2c_v \|\mathcal{E}\|_{\text{op}}}{d} + \frac{4 \|\mathcal{E}\|_{\text{op}}}{d} + \frac{2 \|\mathcal{E}\|_{\text{op}}^2}{d^2} \right) \sum_{i=0}^{k-1} (c_u c_v)^i$$

As before, this implies convergence of the non-stochastic error at a rate geometric in $c_u c_v$. In the $k \rightarrow \infty$ limit, this becomes:

$$\begin{aligned}
|\sin \theta_{\mathbf{u}_k}| &\leq \frac{1}{1 - c_u c_v} \left(\frac{2c_v \|\mathcal{E}\|_{\text{op}}}{d} + \frac{4 \|\mathcal{E}\|_{\text{op}}}{d} + \frac{2 \|\mathcal{E}\|_{\text{op}}^2}{d^2} \right) \\
&\leq \frac{6 \frac{\|\mathcal{E}\|_{\text{op}}}{d} + 2 \frac{\|\mathcal{E}\|_{\text{op}}^2}{d^2}}{1 - c_u c_v} \\
&\leq \frac{6 \frac{\|\mathcal{E}\|_{\text{op}}}{d} + 2 \frac{\|\mathcal{E}\|_{\text{op}}}{d}}{1 - c_u c_v} \\
&= \frac{8 \|\mathcal{E}\|_{\text{op}}}{d(1 - c_u c_v)}
\end{aligned}$$

matching the $\theta_{\mathbf{v}_k}$ bounds given above.

The analysis in this section extends naturally to the general rank- r case: algebraically, it is simpler to work with the root mean Frobenius error $\|\sin \Theta(\mathbf{V}_*, \mathbf{V}^{(k+1)})\|_F / \sqrt{r}$ rather than the total Frobenius error to eliminate the extra factor of \sqrt{r} . Under this scaling, the right hand sides of each step match those given above. The resulting error bound is then:

$$\|\sin \Theta(\mathbf{v}_*, \mathbf{v}^{(k)})\|_F \leq \frac{8\sqrt{r} \|\mathcal{E}\|_{r\text{-op}}}{d(1 - c_u c_v)} \text{ as } k \rightarrow \infty$$

Finally, to get the MSE bounds given in the statement of this theorem, we recall that

$$\sin \angle(\mathbf{u}_*, \hat{\mathbf{u}}) = c \iff \min_{\epsilon = \pm 1} \frac{\|\epsilon \mathbf{u}^* - \hat{\mathbf{u}}\|_2}{\sqrt{2}} = c$$

Hence,

$$\begin{aligned}\min_{\epsilon=\pm 1} \|\epsilon \mathbf{u}^* - \hat{\mathbf{u}}\|_2 &\leq \frac{8\sqrt{2} \|\mathcal{E}\|_{\text{op}}}{d(1 - c_u c_v)} \\ \min_{\epsilon=\pm 1} \|\epsilon \mathbf{v}^* - \hat{\mathbf{v}}\|_2 &\leq \frac{8\sqrt{2} \|\mathcal{E}\|_{\text{op}}}{d(1 - c_u c_v)}\end{aligned}$$

Or in the rank- r case: there exists an orthogonal matrix \mathbf{O} such that:

$$\|\mathbf{V}^* \mathbf{O} - \hat{\mathbf{V}}\|_F \leq \frac{8\sqrt{2r} \|\mathcal{E}\|_{r\text{-op}}}{d(1 - c_u c_v)}$$

The passage from $\sin(\cdot)$ bounds to ℓ_2 error is standard: see, e.g., the discussion of Equation A5 in the paper by Yu, Wang, and Samworth [2].

IV. Condition Checking. In the previous section, we assumed in Equation (A3) that we had a “shrinkage factor” of at least $\max(c_u, c_v) < 1$ at each iteration. This assumption may appear strenuous but it follows naturally from the assumption on the initialization \mathbf{u} in the statement of our theorem. Specifically, we can combine an initialization condition with the contraction condition of Equation (A4) to ensure that we stay in the “contraction interval” given by $|\sin \theta| \in [0, 2 \tan^{-1}(0.5)]$. Specifically, we note that at iteration k , we have

$$\begin{aligned}|\sin \theta_{v_k}| &= (c_u c_v)^k |\sin \theta_{v_1}| + \left(\frac{2c_v \|\mathcal{E}\|_{\text{op}}}{d} + \frac{4 \|\mathcal{E}\|_{\text{op}}}{d} + \frac{2 \|\mathcal{E}\|_{\text{op}}^2}{d^2} \right) \frac{1 - (c_u c_v)^k}{1 - c_u c_v} \\ &\leq |\sin \theta_{v_1}| + \frac{8 \|\mathcal{E}\|_{\text{op}}}{d(1 - c_u c_v)} \quad \text{for all } k = 1, 2, 3, \dots\end{aligned}$$

Hence, if we want to stay in the contraction interval for all k it suffices to have

$$|\sin \theta_{v_1}| + \frac{8 \|\mathcal{E}\|_{\text{op}}}{d(1 - c_u c_v)} \leq 2 \tan^{-1}(0.5)$$

or, equivalently,

$$|\sin \theta_{v_1}| \leq 2 \tan^{-1}(0.5) - \frac{8 \|\mathcal{E}\|_{\text{op}}}{d(1 - c_u c_v)}.$$

To connect this to our initialization condition on \mathbf{u}_0 , we use Equation (A1) one final time to find that it suffices to have

$$2|1 - \cos \theta_{u_0}| + \frac{2 \|\mathcal{E}\|_{\text{op}}}{d} \leq 2 \tan^{-1}(0.5) - \frac{8 \|\mathcal{E}\|_{\text{op}}}{d(1 - c_u c_v)}.$$

Rearranging this, we obtain the initialization condition on \mathbf{u} :

$$|1 - \cos \theta_{u_0}| \leq \tan^{-1}(0.5) - \frac{5 \|\mathcal{E}\|_{\text{op}}}{d(1 - c_u c_v)},$$

letting $c = c_u c_v$ be the arbitrary constant in the statement of the lemma.

The general rank r -case follows immediately. □

Next, we prepare to transfer from the “deterministic” Lemma 1 to the more familiar stochastic setting of Theorems 1 and 2 via a standard concentration bound on $\|\mathcal{E}\|_{r\text{-op}}$. Our key tool is Proposition 2, which we restate and prove with more detail here for convenience:

Proposition 2. *The semi-symmetric operator norm, $\|\mathcal{X}\|_{r\text{-op}} = \max_{\mathbf{u}, \mathbf{V} \in \mathbb{B}^T \times \mathcal{V}^{p \times r}} |[\mathcal{X}, \mathbf{V}]^T \mathbf{u}|$ can be bounded above by $r\sqrt{T} \max_i \lambda_{\max}(\mathcal{X}_{\cdot i})$. Furthermore, if the elements of \mathcal{X} are independently σ^2 -sub-Gaussian, subject to symmetry constraints, we have*

$$\|\mathcal{X}\|_{r\text{-op}} \leq cr\sqrt{T}\sigma \left(\sqrt{p} + \sqrt{\log T} + \delta \right)$$

with probability at least $1 - 4e^{-\delta^2}$, for some absolute constant c .

Proof. For the deterministic bound,

$$\|\mathcal{X}\|_{r\text{-op}} \leq k\sqrt{T} \max_i |\lambda_{\max}(\mathcal{X}_{\cdot i})|,$$

we note that

$$\begin{aligned}
\|\mathcal{X}\|_{r\text{-op}} &= \max_{\mathbf{u}, \mathbf{V} \in \mathbb{B}^T \times \mathcal{V}^{p \times r}} |\langle [\mathcal{X}; \mathbf{V}], \mathbf{u} \rangle| \\
&= \max_{\mathbf{u} \in \mathbb{B}^T, \mathbf{V} \in \mathcal{V}^{p \times r}} |\langle \text{Tr}(\mathbf{V}^T \mathcal{X}_{..i} \mathbf{V})_i, \mathbf{u} \rangle| \\
&\leq \max_{\mathbf{u} \in \mathbb{B}^T, \mathbf{V}_i \in \mathcal{V}^{p \times r}} |\langle \text{Tr}(\mathbf{V}_i^T \mathcal{X}_{..i} \mathbf{V}_i)_i, \mathbf{u} \rangle| \\
&= \max_{\mathbf{u} \in \mathbb{B}^T, \mathbf{V}_i \in \mathcal{V}^{p \times r}} \left| \left\langle \left(\sum \lambda_{\max:r}(\mathcal{X}_{..i}) \right)_i, \mathbf{u} \right\rangle \right| \\
&\leq r \max_{\mathbf{u} \in \mathbb{B}^T} |\langle (\lambda_{\max}(\mathcal{X}_{..i}))_i, \mathbf{u} \rangle|
\end{aligned}$$

where the first inequality follows by allowing different \mathbf{V}_i for each slice of \mathcal{X} , which can be independently set to the leading r -eigenvectors of $\mathcal{X}_{..i}$, so that the trace is then given by the sum of the top r eigenvalues of the i^{th} slice. The second inequality follows by bounding the sum by r times the maximum eigenvalue. The maximum here is obtained by $\mathbf{u} \propto (\lambda_{\max}(\mathcal{X}_{..i}))_i$ and gives the value $\|(\lambda_{\max}(\mathcal{X}_{..i}))_i\|_2$. Because the elements of this random vector are not mean-zero, this quantity is slightly cumbersome to bound. An acceptable bound can be obtained by recalling that $\|\mathbf{x}\|_2 \leq \sqrt{T}\|\mathbf{x}\|_\infty$ for any $\mathbf{x} \in \mathbb{R}^T$ and then bounding the maximum element. Specifically, we have

$$\begin{aligned}
\|\mathcal{X}\|_{r\text{-op}} &\leq r \|(\lambda_{\max}(\mathcal{X}_{..i}))_i\|_2 \\
&\leq r\sqrt{T} \|(\lambda_{\max}(\mathcal{X}_{..i}))_i\|_\infty \\
&= r\sqrt{T} \max_i \lambda_{\max}(\mathcal{X}_{..i})
\end{aligned}$$

Next, to get the stochastic claim, we need to control $\lambda_{\max}(\mathcal{X}_{..i})$ for each i and then apply a union bound to control $\max_i \lambda_{\max}(\mathcal{X}_{..i})$. This follows straight-forwardly from well-known bounds on the operator norm of sub-Gaussian random matrices. Specifically, note that each slice of \mathcal{X} ($\mathcal{X}_{..i}$) is a symmetric matrix with σ^2 -sub-Gaussian entries. Standard results allow us to characterize the operator norm quite accurately: specifically, we have, for fixed i ,

$$\|\mathcal{X}_{..i}\|_{\text{op}} \lesssim \sigma(\sqrt{p} + u)$$

with probability at least $1 - 4\exp(-u^2)$: see, *e.g.*, Corollary 4.4.8 in the text by Vershynin [3]. Combining this with the eigenvalue bound above, we have

$$P \left\{ \|\mathcal{X}\|_{r\text{-op}} \gtrsim \sigma r \sqrt{T} (\sqrt{p} + u) \right\} \leq TP \left\{ \|\mathcal{X}_{..1}\|_{\text{op}} \gtrsim \sigma(\sqrt{p} + u) \right\}$$

by a standard union bound (Boole's inequality) applied to the T independent slices of \mathcal{X} .¹ Standard manipulations then yield:

$$\begin{aligned}
P \left\{ \|\mathcal{X}_{..1}\|_{\text{op}} \lesssim \sigma(\sqrt{p} + u) \right\} &\geq 1 - 4e^{-u^2} \\
1 - P \left\{ \|\mathcal{X}_{..1}\|_{\text{op}} \lesssim \sigma(\sqrt{p} + u) \right\} &< 1 - \left[1 - 4e^{-u^2} \right] \\
P \left\{ \|\mathcal{X}_{..1}\|_{\text{op}} \gtrsim \sigma(\sqrt{p} + u) \right\} &< 4e^{-u^2}
\end{aligned}$$

Hence,

$$P \left\{ \|\mathcal{X}\|_{r\text{-op}} \gtrsim \sigma r \sqrt{T} (\sqrt{p} + u) \right\} < 4Te^{-u^2}$$

or equivalently

$$P \left\{ \|\mathcal{X}\|_{r\text{-op}} \lesssim \sigma r \sqrt{T} (\sqrt{p} + u) \right\} \geq 1 - 4e^{-u^2 + \log T}.$$

Letting $u = \sqrt{\delta^2 + \log T} \Leftrightarrow -u^2 + \log T = -\delta^2$, we obtain the bound

$$P \left\{ \|\mathcal{E}\|_{r\text{-op}} \lesssim \sigma r \sqrt{T} \left(\sqrt{p} + \sqrt{\delta^2 + \log T} \right) \right\} \geq 1 - 4e^{-\delta^2}.$$

Finally, recalling that $\sqrt{a^2 + b} \leq a + \sqrt{b}$ for all $a, b > 1$, we have

$$P \left\{ \|\mathcal{E}\|_{r\text{-op}} \lesssim \sigma r \sqrt{T} \left(\sqrt{p} + \sqrt{\log T + \delta} \right) \right\} \geq 1 - 4e^{-\delta^2}. \quad \square$$

¹Let A_i be the event $\|\mathcal{X}_{..i}\|_{\text{op}} \gtrsim r\sigma(\sqrt{p} + u)$. Then $A = \bigcup_i A_i$ is the event $\|\mathcal{X}\|_{r\text{-op}} \gtrsim r\sigma(\sqrt{p} + u)$ and Boole's inequality gives us:

$$P(A) \leq \sum_i P(A_i) = TP(A_1)$$

with the last inequality following from independence.

With these two results, we are now ready to prove Theorems 1 and 2 which we restate here for convenience of the reader:

Theorem 1. *Suppose \mathcal{X} is generated from the semi-symmetric model described above (1) with elements of \mathcal{E} each independently σ^2 -sub-Gaussian, subject to symmetry constraints. Suppose further that the initialization \mathbf{u}_0 satisfies*

$$|1 - \langle \mathbf{u}_0, \mathbf{u}_* \rangle| \leq \tan^{-1}(0.5) - \frac{5 \|\mathcal{E}\|_{r\text{-op}}}{d(1-c)}$$

for some arbitrary $c < 1$. Then, the output of Algorithm 1 applied to \mathcal{X} satisfies the following

$$\min_{\mathbf{O} \in \mathcal{V}^{r \times r}} \frac{\|\mathbf{V}^* - \hat{\mathbf{V}}\mathbf{O}\|_2}{\sqrt{pr}} \lesssim \frac{\sigma r \sqrt{T}}{d(1-c)}$$

with high probability and where \lesssim denotes an inequality holding up to a universal constant factor and a term scaling as $\sqrt{\log T}$.

Theorem 2. *Under the same conditions as Theorem 1, the output of Algorithm 1 applied to \mathcal{X} satisfies*

$$\min_{\epsilon = \pm 1} \|\epsilon \mathbf{u}_* - \hat{\mathbf{u}}\| / \sqrt{T} \lesssim \frac{\sigma r \sqrt{p}}{d(1-c)}$$

with high probability and \lesssim is as before.

Proof. Under the stated conditions, Lemma 1 implies

$$\begin{aligned} \min_{\epsilon = \pm 1} \|\epsilon \mathbf{u}^* - \hat{\mathbf{u}}\|_2 &\leq \frac{8\sqrt{2} \|\mathcal{E}\|_{r\text{-op}}}{d(1-c)} \\ \|\mathbf{V}^*\mathbf{O} - \hat{\mathbf{V}}\|_F &\leq \frac{8\sqrt{2}r \|\mathcal{E}\|_{r\text{-op}}}{d(1-c)} \end{aligned}$$

so long as $\|\mathcal{E}\|_{r\text{-op}} < d$ and

$$|1 - \langle \mathbf{u}_0, \mathbf{u}_* \rangle| \leq \tan^{-1}(0.5) - \frac{5 \|\mathcal{E}\|_{r\text{-op}}}{d(1-c)}$$

for some arbitrary $c < 1$. Furthermore, under the same conditions, Proposition 2 applied to \mathcal{E} implies that $\|\mathcal{E}\|_{r\text{-op}} \lesssim \sigma r \sqrt{T} (\sqrt{p} + \sqrt{\log T} + \delta)$ with probability at least $1 - 4e^{-\delta^2}$. Substituting this into the error bounds we have:

$$\begin{aligned} \min_{\epsilon = \pm 1} \|\epsilon \mathbf{u}^* - \hat{\mathbf{u}}\|_2 &\lesssim \frac{\sigma r \sqrt{T} (\sqrt{p} + \sqrt{\log T} + \delta)}{d(1-c)} \\ \|\mathbf{V}^*\mathbf{O} - \hat{\mathbf{V}}\|_F &\lesssim \frac{\sqrt{r} \sigma r \sqrt{T} (\sqrt{p} + \sqrt{\log T} + \delta)}{d(1-c)}. \end{aligned}$$

If we normalize the right hand side of each quantity to “root mean squared error” instead of total ℓ_2 error, we have:

$$\begin{aligned} \min_{\epsilon = \pm 1} \|\epsilon \mathbf{u}^* - \hat{\mathbf{u}}\|_2 / \sqrt{T} &\lesssim \frac{\sigma r \sqrt{T} (\sqrt{p} + \sqrt{\log T} + \delta)}{d \sqrt{T} (1-c)} \approx \frac{\sigma \sqrt{p}}{d(1-c)} \\ \|\mathbf{V}^*\mathbf{O} - \hat{\mathbf{V}}\|_F / \sqrt{pr} &\lesssim \frac{\sigma r \sqrt{T} (1 + \sqrt{(\log T)/pr} + \delta/\sqrt{pr})}{d(1-c)} \approx \frac{\sigma \sqrt{T}}{d(1-c)} \end{aligned}$$

with bounds holding with high probability. \square

We highlight that our proof uses the worst-case “ ℓ_2 ” bounds derived using the Davis-Kahan (1970) theorem. These bounds are well-understood and simple to use, particularly in the variant of Yu, Wang, and Samworth [2]. If the maximum elementwise error ($\|\cdot\|_\infty$) is of more use in a specific application, particularly a high-dimensional one, the bounds developed by Fan, Wang, and Zhong [4] and by Damle and Sun [5] may be of use. We also note that we rely on the “worst-case” bound $\|\mathcal{E}\|_{\text{op}}$ throughout instead of using “typical case” bounds: a tighter analysis may be attainable using the tools of Eldridge, Belkin, and Wang [6], at the cost of a significantly more technical proof.

ADDITIONAL REFERENCES

- [1] C. Davis and W. M. Kahan, “The rotation of eigenvectors by a perturbation III,” *SIAM Journal on Numerical Analysis*, vol. 7, no. 1, pp. 1–46, 1970. DOI: [10.1137/0707001](https://doi.org/10.1137/0707001).
- [2] Y. Yu, T. Wang, and R. J. Samworth, “A useful variant of the Davis–Kahan theorem for statisticians,” *Biometrika*, vol. 102, no. 2, pp. 315–323, 2015. DOI: [10.1093/biomet/asv008](https://doi.org/10.1093/biomet/asv008).
- [3] R. Vershynin, *High-Dimensional Probability: An Introduction with Applications in Data Science*, 1st. 2018.

- [4] J. Fan, W. Wang, and Y. Zhong, “An ℓ_∞ eigenvector pertubatiotn bound and its application to robust covariance estimation,” *Journal of Machine Learning Research*, vol. 18, no. 207, pp. 1–42, 2018. [Online]. Available: <https://jmlr.org/papers/v18/16-140.html>.
- [5] A. Damle and Y. Sun, “Uniform bounds for invariant subspace perturbations,” *SIAM Journal on Matrix Analysis and Applications*, vol. 41, no. 3, pp. 1208–1236, 2020. DOI: [10.1137/19M1262760](https://doi.org/10.1137/19M1262760).
- [6] J. Eldridge, M. Belkin, and Y. Wang, “Unperturbed: Spectral analysis beyond Davis-Kahan,” in *ALT 2018: Proceedings of the 29th International Conference on Algorithmic Learning Theory*, vol. 83, 2018, pp. 321–358. [Online]. Available: <https://proceedings.mlr.press/v83/eldridge18a.html>.